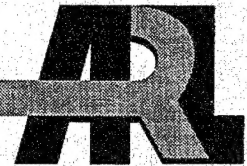ARMY RESEARCH LABORATORY

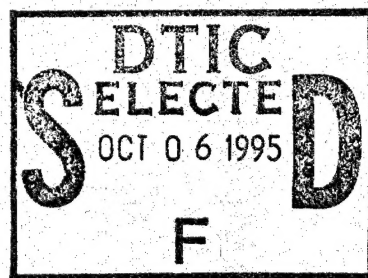# Fast Parabolic Approximations for Acoustic Propagation in the Atmosphere

by David H. Marlin
Battlefield Environment Directorate

DTIC
SELECTED
OCT 0 6 1995
F

19951004 060

DTIC QUALITY INSPECTED 5

NOTICES

Disclaimers

The findings in this report are not to be construed as an official Department of the Army position, unless so designated by other authorized documents.

The citation of trade names and names of manufacturers in this report is not to be construed as official Government indorsement or approval of commercial products or services referenced herein.

Destruction Notice

When this document is no longer needed, destroy it by any method that will prevent disclosure of its contents or reconstruction of the document.

1. AGENCY USE ONLY (Leave blank)	2. REPORT DATE September 1995	3. REPORT TYPE AND DATES COVERED Final	
4. TITLE AND SUBTITLE Fast Parabolic Approximations for Acoustic Propagation in the Atmosphere			**5. FUNDING NUMBERS**
6. AUTHOR(S) David H. Marlin			
7. PERFORMING ORGANIZATION NAME(S) AND ADDRESS(ES) U.S. Army Research Laboratory Battlefield Environment Directorate ATTN: AMSRL-BE-S White Sands Missile Range, NM 88002-5501			**8. PERFORMING ORGANIZATION REPORT NUMBER** ARL-TR-573
9. SPONSORING / MONITORING AGENCY NAME(S) AND ADDRESS(ES) U.S. Army Research Laboratory 2800 Powder Mill Road Adelphi, MD 20783-1145			**10. SPONSORING / MONITORING AGENCY REPORT NUMBER** ARL-TR-573
11. SUPPLEMENTARY NOTES			
12a. DISTRIBUTION / AVAILABILITY STATEMENT Approved for public release; distribution is unlimited.			**12b. DISTRIBUTION CODE** A

13. ABSTRACT (Maximum 200 words)

Parabolic equations can be used to find approximate solutions to the reduced wave equation. By reducing the equation to first order in the range derivative, the solution can be found by marching forward in range. Several numerical techniques can be applied to the solution of the parabolic equation (PE), including finite elements, finite differences, and a Fourier Transform method known as the split-step PE. The split-step solves for each range increment in two steps. First, it propagates forward through a homogenous atmosphere, using the Fourier Transform. It then applies a multiplicative phase correction for index-of-refraction variations. The split-step method leads to a computationally fast model for two reasons: the range steps are several wavelengths, and the Fourier Transform can be evaluated by a Fast Fourier Transform. One of the difficulties encountered in applying the split-step PE to outdoor sound propagation is accommodation of the complex ground impedance. The Green's function PE is a split-step PE which solves for the one-dimensional height–dependant Green's function in a homogenous atmosphere. This Green's function incorporates the complex ground impedance as a complex, angle-dependant plane-wave reflection coefficient.

14. SUBJECT TERMS acoustics, propagation, parabolic equation			15. NUMBER OF PAGES 74
			16. PRICE CODE
17. SECURITY CLASSIFICATION OF REPORT Unclassified	18. SECURITY CLASSIFICATION OF THIS PAGE Unclassified	19. SECURITY CLASSIFICATION OF ABSTRACT Unclassified	20. LIMITATION OF ABSTRACT SAR

i

Contents

Figures

2

1. Introduction

Parabolic approximations to the reduced wave equation have been used extensively in acoustic propagation since the early 1970's [1] and in electromagnetics even earlier [2]. The advantage of a parabolic equation (PE) is that the solution can be marched forward in range; the field at a given range r_0 is not dependant on the field at ranges $r > r_0$. In contrast, the reduced wave equation is elliptic, so the field at range r_0 is dependant on the field at all other ranges. This requires solving a large set of simultaneous equations, a much more demanding problem computationally.

Various PEs have been implemented numerically using finite-differences, finite-elements, and a Fast Fourier Transform (FFT) based method known as the split-step PE. The split-step PE has a significant advantage in that the range step typically is on the order of tens of wavelengths as opposed to tenths of a wavelength for the finite-element and finite-difference models. This makes the split-step much faster, usually by at least one order of magnitude.

The underwater acoustic community was the first to apply the PE, including the split-step, to the acoustic propagation problem. The biggest problem faced in adapting the underwater models to the problem of atmospheric propagation is accommodation of the air-ground boundary. The Green's function parabolic equation (GFPE) [3] is the first split-step PE to include a complex-impedance surface. The purpose of this report is to present a theoretical development of PEs in general, culminating in a detailed description of the GFPE. It brings together theory from a number of sources in a cohesive manner with consistent notation. It is the first in a series of three reports on the GFPE. The second report, *A Sensitivity Study of the Green's Function Parabolic Equation*, examines the sensitivity of the GFPE to the input parameters and presents an approach to the automated selection of several of the parameters based on the sound speed profile. The third report, *A Users Guide to the Green's Function Parabolic Equation*, gives a brief review of the first two and describes the user interface from a more user oriented, less theoretical point of view.

Section 2 derives the reduced wave equation, the starting point for parabolic approximations. Section 3 presents the original narrow-angle PE, followed by

a discussion of the general split-step approach and some wide-angle approximations. Section 4 applies the split-step technique to the problem of the air-ground interface, leading to the GFPE. Section 5 gives examples of the output of the GFPE, along with some comparisons to another outdoor sound propagation model, the Fast Field Program (FFP).

6

2. The Reduced Wave Equation for Acoustic Propagation

Begin with two conservation equations from fluid mechanics: the conservation of mass,

$$\frac{\partial \rho}{\partial t} + \nabla \cdot (\rho V) = 0, \tag{1}$$

and the conservation of momentum, neglecting viscosity[*],

$$\frac{\partial}{\partial t}(\rho V) + \nabla P = 0 \tag{2}$$

where

ρ = the density of the fluid
P = the pressure
V = the fluid velocity.

Each is, in general, a function of position and time. Furthermore, P is assumed to have some functional dependance on density and entropy S,

$$P = P(\rho, S). \tag{3}$$

Acoustic disturbances modeled by PEs involve very small fluctuations from ambient levels, so the following assumptions are made:

$$\rho = \rho_0 + \rho', \ P = p_0 + p', \tag{4}$$

---

[*]For the acoustic phenomenon discussed here, the effects of viscosity are negligible. In a more general setting, viscosity may be important.

with

$$\frac{|\rho'|}{\rho_0}, \frac{|p'|}{p_0}, \|\vec{V}\| \ll 1 . \tag{5}$$

The primed variables are the acoustic fluctuations, while the subscripts indicate ambient quantities. Note that the total velocity is assumed to be small. The PEs discussed here assume an ambient wind velocity of zero. Inserting equation (4) into the conservation laws and neglecting products of small quantities yields the linearized conservation laws

$$\frac{\partial \rho'}{\partial t} + \rho_0 \nabla \cdot \vec{V} = 0 \tag{6}$$

and

$$\rho_0 \frac{\partial \vec{V}}{\partial t} + \nabla p' = 0. \tag{7}$$

Small amplitude sound propagation is generally isentropic, so that

$$P = P(\rho). \tag{8}$$

This can be linearized around the point ρ_0,

$$p' = c^2 \rho', \ c^2 = \frac{\partial P(\rho)}{\partial \rho}\bigg|_{\rho = \rho_0}. \tag{9}$$

Equations (6), (7), and (9) can then be solved for p', resulting in the acoustic wave equation

$$\nabla^2 p' - \frac{1}{c^2} \frac{\partial^2 p'}{\partial t^2} = 0, \tag{10}$$

where

$$c = c(\vec{x}) = \text{the sound speed.}$$

8

The next step is to assume a source periodic in time, with angular frequency ω. This can be expected to give pressure fluctuations of the form

$$p'(\vec{x},t) = p(\vec{x})e^{-i\omega t}, \tag{11}$$

so that p satisfies the reduced wave equation

$$\nabla^2 p + k^2 p = 0, \tag{12}$$

where

$$k = \omega/c.$$

Using cylindrical coordinates (figure 1) and assuming the pressure field is independent of θ leads to

$$\frac{\partial^2 p}{\partial r^2} + \frac{1}{r}\frac{\partial p}{\partial r} + \frac{\partial^2 p}{\partial z^2} + k^2 p = 0. \tag{13}$$
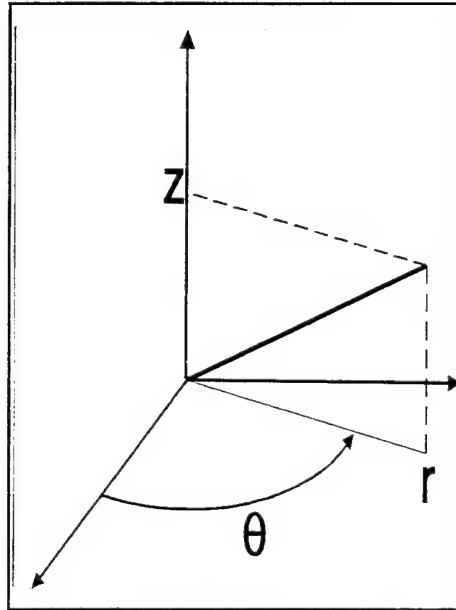
Figure 1.   Cylindrical coordinates used by the PE.

It is well known that a cylindrical wave decreases in amplitude as $r^{1/2}$. To separate this cylindrical spreading loss from other effects, define u by

$$p(r,z) = r^{-\frac{1}{2}} u(r,z). \tag{14}$$

Then u satisfies the reduced wave equation

$$\frac{\partial^2 u}{\partial r^2} + \frac{\partial^2 u}{\partial z^2} + (k^2 + \frac{1}{4r^2})u = 0. \tag{15}$$

Finally, assume $(kr)^2 \gg 1$, which gives rise to

$$\frac{\partial^2 u}{\partial r^2} + \frac{\partial^2 u}{\partial z^2} + k^2 u = 0. \tag{16}$$

Equation (16) is the reduced wave equation describing acoustic propagation far from the source. It is the starting point for the parabolic approximations of the following sections.

3. An Overview of Parabolic Approximations

In the development that follows, the wavenumber k is assumed independent of r, but is allowed to vary with z. In practice, parabolic models are used in weakly range dependant environments. In that case, some of the results below become approximations rather than exact representations. This is pointed out where it occurs. It turns out that the approximations are generally good, and the models yield good results if the range dependance is not too drastic.

3.1 The Narrow-Angle Approximation

The first use of a PE for acoustic propagation was that of Tappert and Hardin [1], who invoked the restriction to narrow propagation angles. Their model is presented in this section.

Begin by expressing u as the product of a horizontal plane wave of wavenumber k_0 and an envelope Ψ,

$$u(r,z) = \Psi(r,z)e^{ik_0 r} \tag{17}$$

where

$k_0 = \omega/c_0$ for some reference sound speed c_0.

Note that $\Psi = |u|$ only when $k \equiv k_0$, which can only occur in a homogenous medium. Substitution of this into the reduced wave equation (16) yields

$$\frac{\partial^2 \Psi}{\partial r^2} + 2ik_0\frac{\partial \Psi}{\partial r} + \frac{\partial^2 \Psi}{\partial z^2} + (k^2 - k_0^2)\Psi = 0. \tag{18}$$

This can easily be made into a PE by omitting the second partial derivative of Ψ with respect to r,

$$2ik_0\frac{\partial \Psi}{\partial r} + \frac{\partial^2 \Psi}{\partial z^2} + (k^2 - k_0^2)\Psi = 0. \tag{19}$$

But when, if ever, is this justified? A sufficient condition is

$$\left|\frac{\partial^2 \Psi}{\partial r^2}\right| \ll \left|k_0 \frac{\partial \Psi}{\partial r}\right|. \tag{20}$$

For a homogenous atmosphere of wavenumber k_0, this can be interpreted via the Fourier Transform pair at a given $r = r_0$:

$$u(r_0, z) = \frac{1}{2\pi} \int_{-\infty}^{\infty} \hat{u}(r_0, k_z) e^{ik_z z} dk_z, \tag{21}$$

and

$$\hat{u}(r, k_z) = \int_{-\infty}^{\infty} e^{-irk_z} u(r, z) dz. \tag{22}$$

Equation (21) can be viewed as a superposition of plane waves of wavenumber k_0,

$$u(r_0 + \Delta r, z) = \frac{1}{2\pi} \int_{-\infty}^{\infty} \hat{u}(r_0, k_z) e^{i(k_r \Delta r + k_z z)} dk_z, \tag{23}$$

where

$$k_r^2 + k_z^2 = k_0^2$$

$$\Delta r = 0.$$

For nonzero Δr, this represents propagation of u to $r = r_0 + \Delta r$ in a homogenous medium of wavenumber k_0. $\hat{u}(r_0, k_z)$ is the amplitude of the plane wave component whose angle of propagation θ satisfies

$$\cos \theta = \frac{k_r}{k_0}. \tag{24}$$

See figure 2. In terms of the envelope, this becomes

$$\Psi(r_0 + \Delta r,z) = \int_{-\infty}^{\infty} \hat{\Psi}(r_0,k_z) e^{i[(k_r - k_0)\Delta r + k_z z]} dk_z. \tag{25}$$
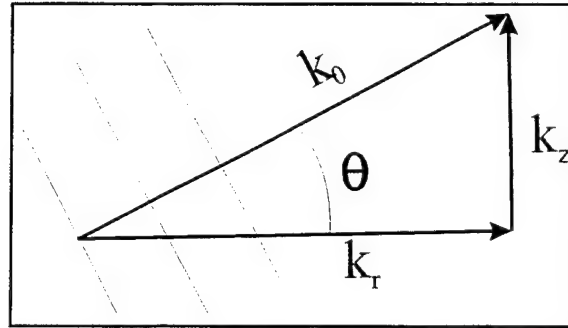
Figure 2. **Wavenumbers and propagation of plane wave components.**

Applying the sufficient condition of equation (20) with respect to Δr gives rise to $|k_r - k_0| \ll k_0$, or

$$\cos\theta \approx 1, \tag{26}$$

hence, the name narrow-angle approximation. In the case of a nonhomogenous atmosphere, the wavenumber variations will introduce wavefront perturbations so equation (25) does not apply. However, in most cases, the perturbations are very small and the wavefronts are still locally approximately planar. Thus, equation (20) is still roughly satisfied by the narrow-angle condition of equation (26). More is said about this in sections 3.3 and 3.4.

3.2 Operators and the Split-Step PE

A more general approach to the PE involves approximations of a certain differential operator, which will be considered next. But first, it is interesting to observe that the term PE is really a misnomer, because most of the operator approximations result in equations that are not parabolic. However, this paper follows custom and continues to use the name parabolic for equations in this class. Also, be aware that frequent use is made of various representations for

13

functions of an operator, without mathematical justification. The formal manipulations are well defined, and the results are valid only for operators satisfying certain unstated conditions. No attempt is made to prove the operators involved satisfy necessary or sufficient conditions. The ultimate justification is empirical; the final results agree well with experimental data and other models.

Begin by expressing equation (16) in operator notation,

$$[\frac{\partial^2}{\partial r^2} + k_0^2 Q]u = 0, \tag{27}$$

where

$$Q = n^2 + \frac{1}{k_0^2} \frac{\partial^2}{\partial z^2}, \tag{28}$$

$n = k/k_0$ = the acoustic index of refraction.

Because k, and therefore n, is independent of r, equation (27) can be factored as follows:

$$(\frac{\partial}{\partial r} + ik_0\sqrt{Q})(\frac{\partial}{\partial r} - ik_0\sqrt{Q})\ u = 0. \tag{29}$$

The left and right factors represent inwardly and outwardly propagating waves, respectively. If k depends on r, the partial derivative with respect to r does not commute with Q, so the factorization is only an approximation.

Interest is in the waves propagating outward from the source, so only the right term is considered,

$$\frac{\partial u}{\partial r} = ik_0\sqrt{Q}\ u. \tag{30}$$

14

The formal solution to this equation is [4]

$$u(r+\Delta r,z) = e^{i\Delta r k_0 \sqrt{Q}} u(r,z).$$

(31)

Note the similarity to the ordinary differential equation

$$\frac{dx}{dt} = \alpha x ,$$

(32)

which has the solution

$$x(t+t_0) = e^{\alpha t} x (t_0).$$

(33)

The difference of course is that the exponential on the right side of equation (31) is a differential operator. The essence of the split-step technique involves approximations of the square root

$$\sqrt{Q} = (n^2 + \frac{1}{k_0^2}\frac{\partial^2}{\partial z^2})^{\frac{1}{2}}$$

$$= (1 + \epsilon + \mu)^{\frac{1}{2}},$$

(34)

where

$$\epsilon = n^2 - 1$$

(35)

$$\mu = \frac{1}{k_0^2}\frac{\partial^2}{\partial z^2}.$$

(36)

The general technique is to linearly separate, or *split* the operators μ and ϵ as

$$\sqrt{Q} \approx \Phi = A(\mu) + B(\epsilon),$$

(37)

15

then write

$$e^{i\Delta r k_0 \sqrt{Q}} \approx e^{i\frac{\Delta r}{2}k_0 A} e^{i\Delta r k_0 B} e^{i\frac{\Delta r}{2}k_0 A}. \tag{38}$$

The symmetric splitting of the exponential is exact only when A and B commute, which will not occur if k varies with z. However, it may still prove to be a good approximation, as is discussed in the next section.

This split-step operator has a simple interpretation. A is independent of ε and therefore n, so the exponential terms in A represent propagation through a homogenous atmosphere. All of the variation in n occurs in the exponential term containing B, and B is a multiplicative operator. Thus, the operators in equation (38) represent propagation through a homogenous atmosphere a distance of $\Delta r/2$, followed by a multiplicative phase correction caused by variations in k, followed by another propagation through a homogenous atmosphere a distance of $\Delta r/2$.

In practice, split-step PEs are usually implemented using a nonsymmetric splitting,

$$e^{i\Delta r k_0 \sqrt{Q}} \approx e^{i\Delta r k_0 A} e^{i\Delta r k_0 B}. \tag{39}$$

The field is initially propagated through free space a distance of $\Delta r/2$ and then alternately phase corrected and stepped forward by Δr. It turns out that the error caused by noncommutativity of A and B is reduced by using a symmetric splitting [5], but past the first $\Delta r/2$ step, the symmetric and nonsymmetric splittings yield the same result, because $e^{i\Delta r k_0 A} = e^{i\frac{\Delta r}{2}k_0 A} e^{i\frac{\Delta r}{2}k_0 A}$. The real issue is the approximation of the operator $\sqrt{Q}$.

3.3   Some Wide-Angle Approximations

Several approximations have been discussed in the literature [6,7,8]. One consists of taking the linear terms in the formal series for the square root of $1 + x$.

16

$$\sqrt{Q} \approx \Phi_N = 1 + \frac{1}{2}\epsilon + \frac{1}{2}\mu. \tag{40}$$

Another approximation, originally suggested by Tappert [6], is

$$\sqrt{Q} \approx \Phi_G = (1 + \mu)^{\frac{1}{2}} + \frac{1}{2}\epsilon. \tag{41}$$

This will be referred to as the GFPE approximation because it is used by Gilbert in the GFPE discussed in the next section.

The wide-angle approximation of Feit and Fleck [7] is

$$\sqrt{Q} \approx \Phi_W = (1 + \mu)^{\frac{1}{2}} + (1 + \epsilon)^{\frac{1}{2}} - 1. \tag{42}$$

These approximations require different restrictions on ϵ and μ. Intuitively, it is necessary to consider the "magnitude" of these operators. However, the usual operator norm,

$$\|A\| = \sup_{|u| = 1} |Au|, \tag{43}$$

will not work. Because μ is unbounded, the supremum is ∞. Instead, as an angle-dependant measure of the magnitude of A, define

$$\|A\|_\theta = |Au|, \tag{44}$$

where u is restricted to unit amplitude plane waves $u = e^{j(k_r r + k_z z)}$ of wavenumber $k_0^2 = k_r^2 + k_z^2$ and propagation angle θ ($\tan \theta = k_z/k_r$).

Note that

$$\|\mu\|_\theta = \sin^2\theta, \tag{45}$$

so μ is small exactly when θ is. Also, $|\epsilon| \ll 1$ is equivalent to $n^2 \approx 1$, or $k \approx k_0$. One would expect that the first approximation (equation (40)) applies for small μ and ϵ, and these are precisely the conditions used for the narrow-angle PE of

section 3.1. It is not difficult to show that equation (40) results in the narrow-angle PE.

More careful analyses of these approximations can be made following Thompson and Chapman [8]. Define the error operators

$$E_N = \Phi_N^2 - Q = \frac{1}{4}(\epsilon^2 + \epsilon\mu + \mu\epsilon + \mu^2), \tag{46}$$

$$E_G = \Phi_G^2 - Q = \epsilon(\frac{1}{4}\epsilon - 1) + \frac{1}{2}\epsilon(1 + \mu)^{\frac{1}{2}} + (1 + \mu)^{\frac{1}{2}}\epsilon, \tag{47}$$

and

$$E_W = \Phi_W^2 - Q = 2[1 - n - (1 + \mu)^{\frac{1}{2}}] + n(1 + \mu)^{\frac{1}{2}} + (1 + \mu)^{\frac{1}{2}}n. \tag{48}$$

Let $n = 1 + \delta n$, and treat δn as a constant. Then

$$\|E_N\|_\theta \leq \frac{1}{4}[|\delta n|(2 + |\delta n|) + \sin^2\theta]^2, \tag{49}$$

$$\|E_G\|_\theta \leq \frac{1}{4}|\delta n|(2 + |\delta n|)[|\delta n|(2 + |\delta n|) + 4|\cos\theta - 1|], \tag{50}$$

and

$$\|E_W\|_\theta \leq 2|\delta n| |\cos\theta - 1|. \tag{51}$$

Figures 3 through 6 show the error bounds as a function of θ and δn, normalized by

$$\|Q\|_\theta = (1 + \delta n)^2 - \sin^2\theta. \tag{52}$$

Figures 3 and 4 vary θ for constant δn of 0.01 and 0.1, respectively. Note that for $\theta = 0$, the wide-angle approximation is exact, while the other bounds are nonzero. As θ increases beyond about 20°, the error bound of the narrow-angle approximation begins to climb rapidly. The GFPE and wide-angle

18

approximations are seen to be valid for larger θ, the difference between the two being the constant bias. Thus, these approximations are considered wide angle.
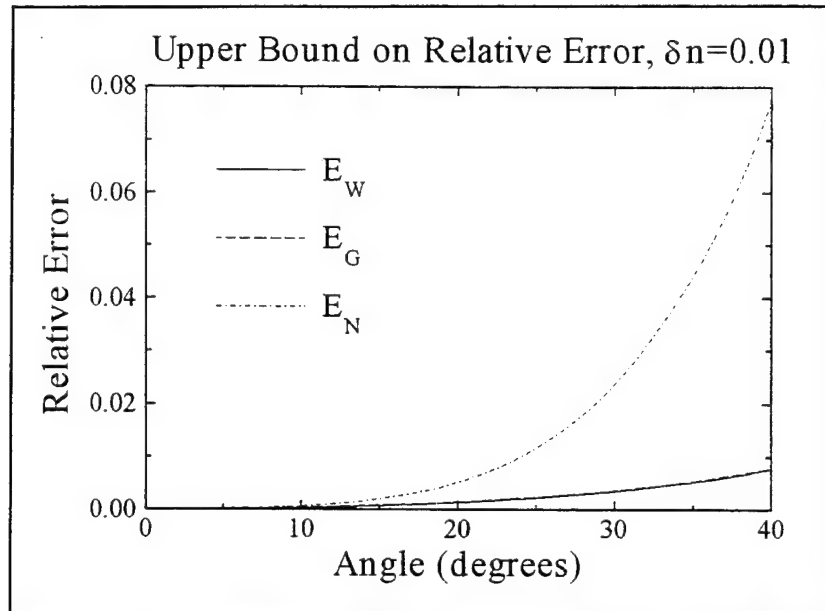
Figure 3. Relative errors as a function of θ for $\delta n = .01$. E_W is wide angle, E_G is GFPE, E_N is narrow angle.
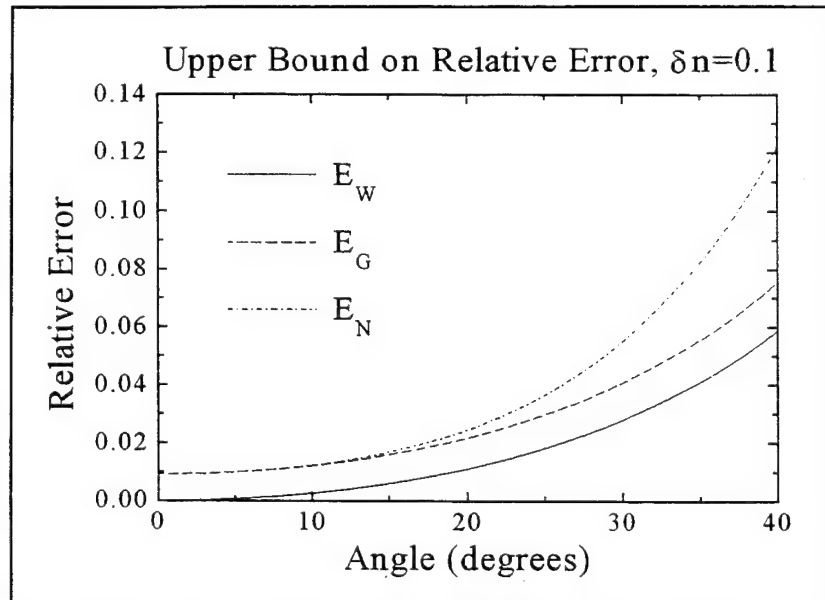
Figure 4. Relative errors as a function of θ for $\delta n = .1$. E_W is wide angle, E_G is GFPE, E_N is narrow angle.

19

Figures 5 and 6 show the normalized errors as a function of δn, for constant θ of 20° and 40°, respectively. The narrow-angle approximation is seen to have a nonzero bound for $\delta n = 0$, while the other two are exact. $\delta n = 0.1$ represents a sound speed variation of approximately 30 m/s, which is larger than almost any variation encountered in the surface boundary layer. Thus, the wide-angle and GFPE approximations are again seen to be good up to a propagation angle of 40°.
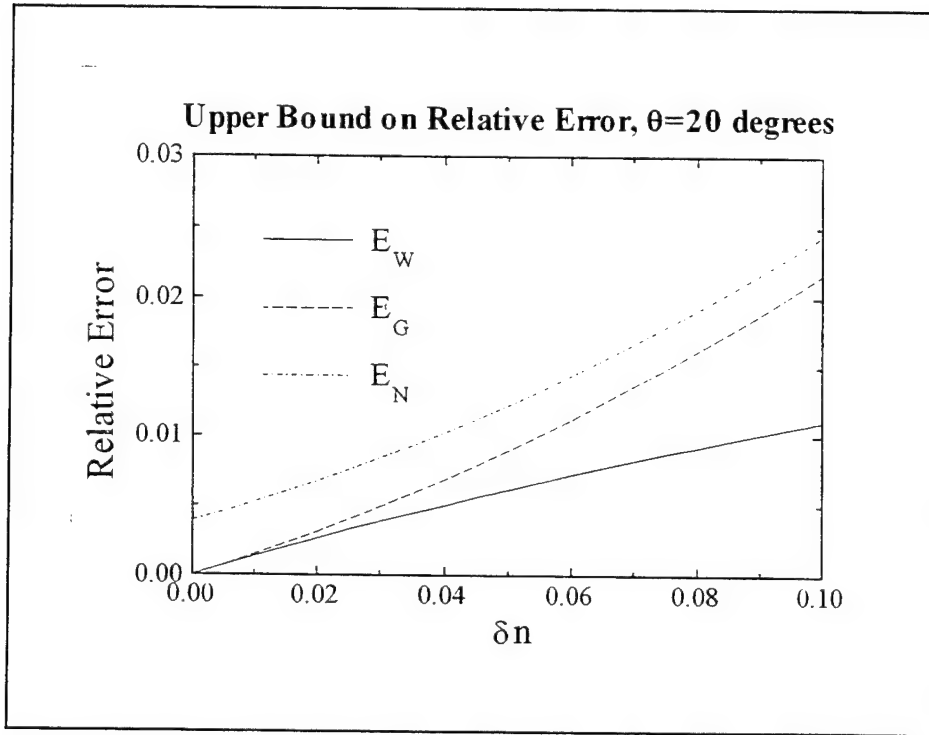
Figure 5. Relative errors as a function of δn for $\theta = 20$. E_W is wide angle, E_G is GFPE, E_N is narrow angle.
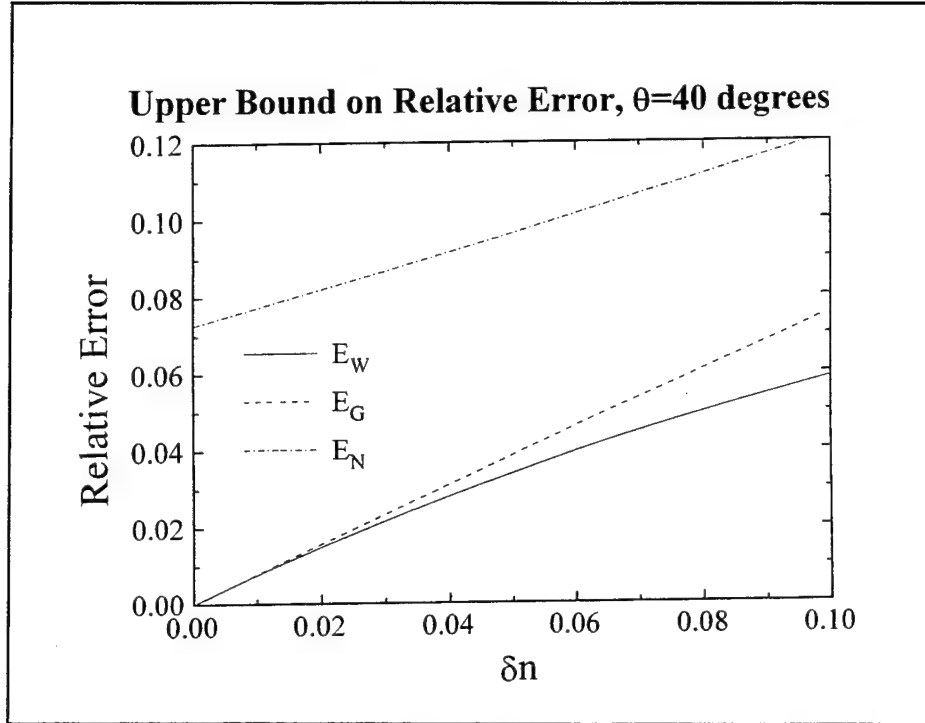
Figure 6. Relative errors as a function of δn for $\theta = 40$. E_W is wide angle, E_G is GFPE, E_N is narrow angle.

McDaniel [9] studied the error associated with the narrow-angle approximation by applying separation of variables to the reduced wave equation and the narrow-angle PE, equation (19). The normal modes for the reduced wave equation in the far field are

$$p_n(r + \Delta r, z) = (\frac{r}{r + \Delta r})^{\frac{1}{2}} e^{ik_n \Delta r} p_n(r, z), \tag{53}$$

while the far field normal modes for the PE are

$$p_n(r + \Delta r, z) = (\frac{r}{r + \Delta r})^{\frac{1}{2}} e^{i\frac{k_n^2 + k_0^2}{2k_0} \Delta r} p_n(r, z). \tag{54}$$

In both cases, k_n is the separation constant, determined by the boundary conditions on the z-dependant equation. This equation is identical for the reduced wave equation and the PE. Thus, the PE is seen to posses a phase error, resulting from the wavenumber

21

$$k_n' = \frac{k_n^2 + k_0^2}{2k_0}, \tag{55}$$

where k_n is the correct wavenumber obtained from the reduced wave equation solution. This results in a phase velocity error in the time-dependant solution

$$c_n' = \frac{2}{c_0}(\frac{1}{c_n^2} + \frac{1}{c_0^2})^{-1} \tag{56}$$

where c_n = the correct modal phase velocity for the wave equation. This error is the result of the narrow-angle approximation; it is not a numerical error associated with any particular numerical implementation technique. The wide-angle and GFPE approximations can be expected to introduce some phase errors as well, although quantitative analyses of these errors are more difficult.

3.4   Implementation Via the FFT

Having considered the error associated with the wide-angle approximation Φ_W, it remains to implement it in a computationally fast algorithm. The key is to observe that for $\varepsilon = 0$, Φ_W gives an exact solution to the Helmholtz equation with constant wavenumber k_0. Recall that with the nonsymmetric splitting,

$$u(r + \Delta r, z) = e^{i\Delta r k_0 \sqrt{Q}} u(r,z) \approx e^{i\Delta r k_0 B} e^{i\Delta r k_0 A} u(r,z), \tag{57}$$

where

$A = \sqrt{1 + \mu}$ for Φ_W

$B = \sqrt{1 + \varepsilon} - 1 = n - 1$ for Φ_W.

Thus, when $\varepsilon = 0$, $(n = 1)$

$$u(r + \Delta r, z) = e^{i\Delta r k_0 \sqrt{Q}} u(r,z) = e^{i\Delta r k_0 A} u(r,z) \tag{58}$$

describes one-way propagation through homogenous space. Section 3.1 shows that this can be represented by

22

$$u(r_0 + \Delta r, z) = \frac{1}{2\pi} \int_{-\infty}^{\infty} \hat{u}(r_0, k_z) e^{i(k_r \Delta r + k_z z)} dk_z, \qquad (59)$$

where

$\hat{u}$ = the Fourier Transform of u with respect to vertical wavenumber k_z

$k_r^2 + k_z^2 = k_0^2.$

But this also represents the inverse Fourier Transform of the quantity $\hat{u} e^{i\Delta r \sqrt{k_0^2 - k_z^2}}$. Thus, for the wide-angle PE, the homogenous propagation is expressed as

$$e^{i\Delta r k_0 A} u(r, z) = \mathscr{F}_{k_z}^{-1} [e^{i\Delta r \sqrt{k_0^2 - k_z^2}} \mathscr{F}_{z'} u(r, z')] , \qquad (60)$$

where

$\mathscr{F}_z$ = the Fourier Transform operator with respect to z

$\mathscr{F}_{k_z}^{-1}$ = the associated inverse transform.

Inclusion of the phase correction term for a nonhomogenous atmosphere yields

$$\begin{aligned} u(r+\Delta r, z) &\approx e^{i\Delta r k_0 B} e^{i\Delta r k_0 A} u(r, z) \\ &= e^{i\Delta r k_0 (n-1)} \mathscr{F}_{k_z}^{-1} [e^{i\Delta r \sqrt{k_0^2 - k_z^2}} \mathscr{F}_{z'} u(r, z')] . \end{aligned} \qquad (61)$$

This is the wide-angle split-step PE. The Fourier Transforms are implemented via an FFT, which can be computed with speed and efficiency using one of the widely available power-of-two algorithms. In practice, the range steps are several wavelengths long, in contrast to finite-element and finite-difference techniques that use range steps much less than a wavelength. The combination of long range steps and FFT is what makes the split-step PE so fast.

Notice that no explicit mention of boundaries such as the ground or water surface has been made. In general, integral transforms are applied so as to explicitly represent the boundary conditions. For the present problem, that would require a transform with respect to range r, so that the boundary condition would be translated to $\hat{u}(k_r,z)$. Instead, the split-step PE applies the transform with respect to z, so that the boundary no longer exists in the wavenumber domain. Thus, the boundary conditions can not be accounted for explicitly; they actually become conditions on the symmetry of $\hat{u}(r,k_z)$.

A condition which can be incorporated is that of a pressure release surface, $u(r,0) = 0$. In this case, the function u can be defined for z < 0 by $u(r,z) = -u(r,-z)$, which forces the pressure release condition. Then the transform is defined for all z, eliminating an explicit boundary condition. This is the method of images, modeling the reflected waves as direct waves propagating upward across the z = 0 boundary. The reflection coefficient is $R \equiv -1$.

Of course, the FFT imposes two boundary conditions, because the transform must be finite in length. The lower boundary can be treated as a pressure release surface by exploiting the relationship between symmetries in the two domains; the reflected spectrum is -1 times the mirror image of the direct spectrum. Because of the periodicity induced by the FFT, this will result in a pressure release surface at the other boundary as well. The unwanted reflections from this surface can be attenuated by introducing an artificial absorption layer near the upper boundary. Care must be taken not to attenuate refracted sound which may reach the detector.

This model works well for underwater acoustics, where it has been used since the early 1970's. The air-water interface is a pressure-release surface (at least for smooth surfaces), and the ocean bottom is generally a thick layer of sediment that strongly attenuates sound with little reflection. However, this is not the case for outdoor sound propagation, as the ground generally is neither a pressure-release surface nor a thick attenuating layer. Thus, the split-step PE needs a formulation that explicitly accommodates more general boundary conditions.

4. Complex Ground Impedance and the GFPE

Reflections from the ground can have a significant effect on the propagating wavefield. Multiple reflections in a downward refracting atmosphere can result in propagation to very great distances. Coherence effects between direct and reflected wavefields can produce interference patterns. To incorporate these effects into a model, it is necessary to accurately represent the ground interaction.

In many cases, the ground can be modeled as a locally reacting surface, using a complex surface impedance [10]. The impedance can easily be incorporated into finite element and finite difference PEs, but the wide-angle split-step PE incorporates only a pressure-release surface, as discussed above. The advantage of the GFPE, as shown below, is that it incorporates a complex-impedance surface, while still allowing implementation via an FFT for speed. It is the combination of these two features that distinguishes the GFPE from previous implementations.

4.1 The Split-Step Approximation

The starting point is again the outgoing component of the reduced wave equation (16),

$$\frac{\partial u}{\partial r} = i k_0 \sqrt{Q} u, \tag{62}$$

where

$$Q = \frac{1}{k_0^2} \frac{\partial^2}{\partial z^2} + n^2. \tag{63}$$

The vertical dependance on height is characterized by

$$k^2(z) = k_0^2 + \delta k^2(z), \tag{64}$$

where the perturbation $\delta k^2(z)$ is assumed small,

$$\frac{|\delta k^2(z)|}{k_0^2} \ll 1. \tag{65}$$

In terms of n and ε, this becomes

$$n^2 = \frac{k^2}{k_0^2} = 1 + \frac{\delta k^2}{k_0^2} = 1 + \varepsilon. \tag{66}$$

The GFPE is a split-step PE with the approximation Φ_G discussed above,

$$\sqrt{Q} \approx (1 + \mu)^{\frac{1}{2}} + \frac{\varepsilon}{2} = (1 + \frac{1}{k_0^2}\frac{\partial^2}{\partial z^2})^{\frac{1}{2}} + \frac{\delta k^2}{2k_0^2}. \tag{67}$$

A nonsymmetric splitting is used, giving rise to the formal solution

$$u(r + \Delta r, z) = e^{i\Delta r k_0 B} e^{i\Delta r k_0 A} u(r,z) = e^{\frac{i\Delta r \delta k^2}{2k_0}} e^{i\Delta r k_0 \sqrt{\tilde{Q}}} u(r,z), \tag{68}$$

where

$$A = (1 + \frac{1}{k_0^2}\frac{\partial^2}{\partial z^2})^{\frac{1}{2}} = \sqrt{\tilde{Q}}. \tag{69}$$

As with the wide-angle split-step PE, this solution first propagates a distance Δr through a homogenous atmosphere of wavenumber k_0, and then applies a phase correction for the nonhomogeneous wavenumber variations. Note that the wide-angle PE and GFPE use the same operator for the homogenous propagation. The distinguishing feature of the GFPE is its incorporation of a

26

complex impedance boundary condition. To do this, a spectral representation is employed to express $e^{i\Delta r k_0 \sqrt{\tilde{Q}}} u$ as the integral of a Green's function.

4.2   The Spectral Representation of an Operator

The spectral form for a function of an operator A is [4]

$$f(A) = \frac{1}{2\pi i} \oint_C f(x) \, [xI - A]^{-1} \, dx, \tag{70}$$

where

C = the boundary of an open set containing the spectrum of A.

The spectrum is defined so that the operator $[xI - A]$ is invertible and bounded everywhere on C and in the region bounded by C. In the present case, the function is $f(x) = e^{i\Delta r k_0 \sqrt{\tilde{Q}}}$, giving rise to

$$e^{i\Delta r k_0 \sqrt{\tilde{Q}}} = \frac{1}{2\pi i} \oint_C e^{i\Delta r k_0 \sqrt{x}} \, [xI - \tilde{Q}]^{-1} \, dx. \tag{71}$$

The change of variables $x = k_r^2/k_0^2$ leads to

$$e^{i\Delta r k_0 \sqrt{\tilde{Q}}} = \frac{1}{\pi i} \oint_{C'} e^{ik_r \Delta r} \, [k_r^2 I - k_0^2 \tilde{Q}]^{-1} k_r \, dk_r. \tag{72}$$

This is an operator, and its action on u, $e^{i\Delta r \sqrt{\tilde{Q}}} u$, may be found by bringing u inside the integral,

$$e^{i\Delta r k_0 \sqrt{\tilde{Q}}} u(r,z) = \frac{1}{\pi i} \oint_{C'} e^{ik_r \Delta r} \, [k_r^2 I - k_0^2 \tilde{Q}]^{-1} u(r,z) \, k_r \, dk_r. \tag{73}$$

Observe that the integrand is no longer operator valued. Defining the function ϕ as

$$\phi(k_r, r, z) = [k_r^2 I - k_0^2 \tilde{Q}]^{-1} u(r,z) \tag{74}$$

leads to

$$e^{i\Delta r k_0 \sqrt{\tilde{Q}}} u(r,z) = \frac{1}{\pi i} \oint_C e^{ik_r \Delta r} \phi(k_r,r,z) k_r dk_r. \tag{75}$$

In terms of the definition of $\tilde{Q}$, the integrand ϕ satisfies the equation

$$(\frac{\partial^2}{\partial z^2} + k_z^2) \phi(k_r,r,z) = -u(r,z), \tag{76}$$

with $k_z^2 = k_0^2 - k_r^2$. This can be solved via a Green's function $G(k_z,z,z')$,

$$\phi(k_r,r,z) = \int_0^\infty G(k_z,z,z') u(r,z') dz', \tag{77}$$

where G satisfies

$$(\frac{\partial^2}{\partial z^2} + k_z^2) G(k_z,z,z') = -\delta(z - z'). \tag{78}$$

All together,

$$e^{i\Delta r k_0 \sqrt{\tilde{Q}}} u(r,z) = \frac{1}{\pi i} \oint_C e^{ik_r \Delta r} \int_0^\infty G(k_z,z,z') u(r,z') dz' k_r dk_r. \tag{79}$$

The next step is to solve for the Green's function, incorporating the complex impedance boundary condition.

4.3 Incorporation of Complex Ground Impedance

The particular form of G depends on the choice of boundary conditions for equation (78). In general, solutions contain direct and reflected terms like $e^{ik_z Z(z,z')}$, where $Z(z,z')$ is a piecewise linear function such as $z + z'$ or $|z - z'|$. Thus, equation (79) constructs the field as a superposition of plane wave components

28

$$e^{i[k_r \Delta r + k_z Z(z,z')]}.$$ (80)

The correct boundary conditions for equation (78) are a radiation condition for large z and the surface boundary condition at $z = 0$.

In general, the surface boundary condition can be quite complicated, describing nonlocal interaction between the air acoustic waves and the ground. A plane wave impinging upon the surface at one point can induce a surface wave that may interact with waves at another location. In many cases, the surface can be modeled as locally reacting. In this case, plane waves incident upon the surface are strongly refracted, so the transmitted energy propagates nearly perpendicular to the surface, producing only local interaction. The boundary condition for this type of surface can be described using surface impedance.

The surface impedance is defined as

$$Z = -\frac{p'}{V_n},$$ (81)

where

p' = the acoustic pressure at the surface

V_n = the outward component of acoustic velocity normal to the surface.

Because the pressure and velocity may not be in phase, Z is generally complex. When the surface is the ground, it is referred to as the complex ground impedance. There are many models available to estimate the ground impedance [10,11]. While many models are based on physical principles, most are somewhat phenomenological or empirical.

Boundary conditions for a differential equation such as equation (78) are generally specified as

$$a\frac{\partial G(r,z)}{\partial z} + bG(r,z) = 0\big|_{z=0},$$ (82)

where $a^2 + b^2 > 0$. Using the linearized conservation of momentum equation (7) and the definitions of Z in equation (81), p in equation (11), and $k_0 = \omega/c_0$, the vertical momentum equation becomes

$$\frac{\partial p'}{\partial z} = -\rho_0 \frac{\partial V_n}{\partial t} = +\frac{\rho_0}{Z} \frac{\partial p'}{\partial t} = -i\frac{\omega \rho_0}{Z}p' = -ik_0\frac{\rho_0 c}{Z}p. \qquad (83)$$

This applies to the Green's function G, which represents acoustic pressure. In terms of the dimensionless quantity $Z_g = \dfrac{Z}{\rho_0 c}$, the boundary condition is

$$\frac{\partial G}{\partial z} + i\frac{k_0}{Z_g}G = 0 \Big|_{z = 0}. \qquad (84)$$

The resulting Green's function is

$$G(k_z, z, z') = \frac{i}{2k_z}[e^{ik_z|z - z'|} + R(k_z)e^{ik_z(z + z')}], \qquad (85)$$

where

$$R(k_z) = \frac{k_z Z_g - k_0}{k_z Z_g + k_0} \qquad (86)$$

is the plane wave reflection coefficient. Substituting this Green's function into equation (79) gives

$$e^{i\Delta r k_0 \sqrt{\bar{Q}}}u(r,z) = \frac{1}{\pi i}\oint_C e^{ik_r \Delta r}\int_0^\infty \frac{i}{2k_z}[e^{ik_z|z - z'|} \qquad (87)$$
$$+ R(k_z)e^{ik_z(z + z')}]u(r,z')\,dz'\,k_r\,dk_r.$$

4.4 Implementation Via the FFT

The final goal is to implement the GFPE via an FFT, as with the wide-angle split-step PE of section 3. Thus, it is necessary to manipulate equation (87) into the form of a Fourier Transform with respect to z, followed by a

multiplication, followed by an inverse transform with respect to a vertical wavenumber. The Green's function is already expressed in terms of z and k_z, but the contour integral is with respect to horizontal wavenumber k_r. Thus, it is necessary to introduce an integration with respect to vertical wavenumber and perform the horizontal wavenumber integration.

Therefore, consider the integral

$$\frac{1}{2\pi} \int_{-\infty}^{\infty} \frac{e^{i\kappa(z - z')}}{\kappa^2 - k_z^2} \, d\kappa, \tag{88}$$

which can be evaluated using the method of residues. The standard technique is to integrate around a closed contour C_a in the complex plane consisting of the interval $[-a,a]$ along the real axis and a semicircle of radius a in the upper or lower half plane $(a > 0)$. The choice of half plane is made to ensure that the integral along the semicircle approaches zero as $a \rightarrow \infty$. Then

$$\frac{1}{2\pi} \int_{-\infty}^{\infty} \frac{e^{i\kappa(z - z')}}{\kappa^2 - k_z^2} \, d\kappa = \pm \lim_{a \to \infty} \frac{1}{2\pi} \int_{C_a} \frac{e^{i\kappa(z - z')}}{\kappa^2 - k_z^2} \, d\kappa. \tag{89}$$

By the residue theorem, the integral on the right side is simply $2\pi i \Sigma$ (residues of poles inside C_a), which in the limit includes all poles in the associated half plane. The sign on the right side of equation (89) depends on which contour is used. The residue theorem requires that the contour be traversed in a counterclockwise direction. If C_a is chosen to fall in the lower half plane, the interval $[-a,a]$ is traversed from a to $-a$, so the negative sign must be used.

To avoid poles on the real axis, k_z is taken as complex with imaginary part $\delta > 0$. This corresponds to absorption, which reduces the amplitude of a propagating waveform by $e^{-\delta z}$. The poles of the integrand occur at $\pm k_z$, with one in the upper half space and one in the lower half space. Thus, only one will be enclosed by C_a. For the case $z - z' > 0$, the contour must fall in the upper half plane, and the resulting residue is

$$(k - k_z)\frac{e^{ik(z - z_0)}}{k^2 - k_z^2}\Big|_{k = k_z} = \frac{e^{ik_z(z - z_0)}}{2k_z}. \tag{90}$$

When $z - z' < 0$, the contour must be in the lower half circle, and the residue there is

$$(k + k_z)\frac{e^{ik(z - z_0)}}{k^2 - k_z^2}\Big|_{k = -k_z} = \frac{e^{-ik_z(z - z_0)}}{-2k_z}. \tag{91}$$

Thus,

$$\frac{1}{2\pi}\int_{-\infty}^{\infty} \frac{e^{i\kappa(z - z')}}{\kappa^2 - k_z^2}\, d\kappa = \frac{i}{2k_z}e^{ik_z|z - z'|}. \tag{92}$$

Similarly,

$$\frac{1}{2\pi}\int_{-\infty}^{\infty} R(\kappa)\frac{e^{i\kappa(z + z')}}{\kappa^2 + k_z^2}\, d\kappa = \frac{i}{2k_z}R(k_z)e^{ik_z(z + z')} - 2i\beta\frac{e^{-i\beta(z + z')}}{\beta^2 - k_z^2}, \tag{93}$$

where

$$\beta = \frac{k_0}{Z_g}. \tag{94}$$

In this case, the contour must always be chosen in the upper half plane because the argument of the exponential is always positive. The reflection coefficient introduces the extra pole at $-\beta$, which will fall in the upper half plane because of the nature of Z_g.

Using equations (92) and (93), the Green's function may be written as

$$g(\kappa,z,z') = \frac{1}{2\pi} \int_{-\infty}^{\infty} \frac{e^{i\kappa(z - z')}}{\kappa^2 - k_z^2} d\kappa + \frac{1}{2\pi} \int_{-\infty}^{\infty} R(\kappa) \frac{e^{i\kappa(z + z')}}{\kappa^2 - k_z^2} d\kappa$$
$$+ 2i\beta \frac{e^{-i\beta(z + z')}}{\beta^2 - k_z^2}, \tag{95}$$

the integrations over height z and vertical wavenumber κ necessary for forward and inverse Fourier Transforms,

$$e^{i\Delta r k_0 \sqrt{\bar{Q}}} u(r,z) = \frac{1}{\pi i} \oint_C e^{ik_r\Delta r} k_r dk_r \int_0^{\infty} [\frac{1}{2\pi} \int_{-\infty}^{\infty} \frac{e^{i\kappa(z - z')}}{\kappa^2 - k_z^2} d\kappa$$
$$+ \frac{1}{2\pi} \int_{-\infty}^{\infty} R(\kappa) \frac{e^{i\kappa(z + z')}}{\kappa^2 - k_z^2} d\kappa + 2i\beta \frac{e^{-i\beta(z + z')}}{\beta^2 - k_z^2}] u(r,z') dz'. \tag{96}$$

Exchanging the order of integration gives equation (97) for the homogenous propagation term:

$$e^{i\Delta r k_0 \sqrt{\bar{Q}}} u(r,z) = \frac{1}{2\pi} \int_{-\infty}^{\infty} e^{i\kappa z} d\kappa \frac{1}{\pi i} \int_C \frac{e^{ik_r\Delta r}}{\kappa^2 - k_z^2} k_r dk_r \int_0^{\infty} e^{-i\kappa z'} u(r,z') dz'$$
$$+ \frac{1}{2\pi} \int_{-\infty}^{\infty} e^{i\kappa z} d\kappa R(\kappa) \frac{1}{\pi i} \int_C \frac{e^{ik_r\Delta r}}{\kappa^2 - k_z^2} k_r dk_r \int_0^{\infty} e^{i\kappa z'} u(r,z') dz' \tag{97}$$
$$+ 2i\beta e^{-i\beta z} \frac{1}{\pi i} \int_C \frac{e^{ik_r\Delta r}}{\beta^2 - k_z^2} k_r dk_r \int_0^{\infty} e^{-i\beta z'} u(r,z') dz'.$$

The Fourier Transforms are clearly visible in the first two lines. The first line represents the direct wave, and the second line is the reflected wave. The third line represents the surface or creeping wave [12]. The homogenous phase multiplication can now be simplified by performing the contour integral

33

$$\frac{1}{\pi i} \int_C \frac{e^{ik_r \Delta r}}{\kappa^2 - k_z^2} k_r \, dk_r. \tag{98}$$

The residue theorem is used again, and the poles are determined by recalling that $k_z^2 = k_o^2 - k_r^2$. The denominator is then $k_r^2 - (k_0^2 - \kappa^2)$, with zeros

$$k_r = \pm \sqrt{k_0^2 - \kappa^2}. \tag{99}$$

At this point, it is necessary to determine whether the poles fall in the spectrum of $\tilde{Q}$. For the moment, assume that the positive pole is enclosed by the contour, so

$$\frac{1}{\pi i} \int_C \frac{e^{ik_r \Delta r}}{\kappa^2 - k_z^2} k_r \, dk_r = e^{i \Delta r \sqrt{k_0^2 - k_z^2}}. \tag{100}$$

The homogenous propagation term then becomes

$$
\begin{aligned}
e^{i \Delta r \sqrt{\tilde{Q}}} u(r,z) &= \frac{1}{2\pi} \int_{-\infty}^{\infty} e^{i\kappa z} \, d\kappa \, e^{i \Delta r \sqrt{k_0^2 - \kappa^2}} \int_0^{\infty} e^{-i\kappa z'} u(r,z') \, dz' \\
&+ \frac{1}{2\pi} \int_{-\infty}^{\infty} e^{i\kappa z} \, d\kappa \, R(\kappa) e^{i \Delta r \sqrt{k_0^2 - \kappa^2}} \int_0^{\infty} e^{i\kappa z'} u(r,z') \, dz' \\
&+ 2i\beta e^{-i\beta z} \, e^{i \Delta r \sqrt{k_0^2 - \beta^2}} \int_0^{\infty} e^{-i\beta z'} u(r,z') \, dz'.
\end{aligned}
\tag{101}
$$

Compare this to the wide-angle split-step PE and recall that the two split-step approximations Φ_W and Φ_G use the same homogenous propagation term $A(\mu)$, with different boundary conditions. As mentioned above, the wide-angle PE implicitly uses a pressure-release boundary condition. In terms of impedance, this is equivalent to $Z_g = 0$, because the pressure is equal to zero. In this case, $R(\kappa) = -1$, and equation (101) agrees exactly with the homogenous propagation part of the wide-angle split-step PE. Thus, it is concluded from physical reasoning that equation (100) is correct and equation (101) does indeed represent the homogenous propagation portion of the GFPE.

34

Adding the nonhomogenous phase correction term yields as the final form for the GFPE

$$
e^{i\Delta r\sqrt{\bar{Q}}}u(r,z) = e^{i\Delta r\frac{\delta k^2}{2k_0}}\{\frac{1}{2\pi}\int_{-\infty}^{\infty}e^{i\kappa z}\,d\kappa\,e^{i\Delta r\sqrt{k_0^2 - \kappa^2}}\int_{0}^{\infty}e^{-i\kappa z'}u(r,z')\,dz'
$$

$$
+ \frac{1}{2\pi}\int_{-\infty}^{\infty}e^{i\kappa z}\,d\kappa\,R(\kappa)\,e^{i\Delta r\sqrt{k_0^2 - \kappa^2}}\int_{0}^{\infty}e^{i\kappa z'}u(r,z')\,dz' \qquad (102)
$$

$$
+ 2i\beta e^{-i\beta z}\,e^{i\Delta r\sqrt{k_0^2 - \beta^2}}\int_{0}^{\infty}e^{-i\beta z'}u(r,z')\,dz'\}\,.
$$

Note the two differences between the GFPE and wide-angle PE. One is the correction factor used for the nonhomogenous sound speed profile; the other is the reflection coefficient. The wide-angle PE assumes a reflection coefficient $R \equiv -1$, which produces no amplitude change and a 180° phase shift. The GFPE reflection coefficient produces angular dependant amplitude and phase changes and also introduces the surface wave term that results from the zero of R.

In practice, the first two lines can be implemented via a single FFT/inverse FFT pair. Note that the GFPE, as with any split-step PE, generates a two-dimensional (2-D) pressure field, because the FFT gives a profile of pressure versus height at each range step. It is generally necessary to interpolate between points to get the field at a specified height.

35

5. Model Comparisons

The FFP [13] is another model in wide use in the atmospheric acoustics community. It is a full-wave model, based on an integral transform of the reduced wave equation. The FFP transforms with respect to range and horizontal wavenumber, thereby preserving the boundary condition and height-dependant sound-speed in the transform domain. As discussed above, the GFPE is an integral transform in height and vertical wavenumber, but incorporation of the boundary conditions and height-dependant sound-speed is not straightforward.

The FFP numerically solves for a height-dependant Green's function in the horizontal-wavenumber domain, then transforms to the range domain. Because of this, the sound-speed profile and ground impedance must be range independent; there is no place for range dependance in the horizontal-wavenumber domain. Thus, it exactly incorporates the height-dependant sound-speed, but the cost is range independence.

In contrast, the Green's function of the GFPE represents a homogenous atmosphere in the vertical-wavenumber domain; the sound-speed variations are handled by an approximation in the spacial domain. The advantage is the sound speed and ground impedance can vary with range.

Figure 8 shows the full 2-D output of the GFPE for the sound-speed profile of figure 7. Note that this profile is a simulated surface duct, not a measured profile. Figure 9 gives a comparison between the FFP and the one-dimensional (1-D) sound pressure level versus range output of the GFPE, again using the profile of figure 7. The frequency for figures 8 and 9 is 20 Hz and the source height is 5 m. The blocky appearance of the 2-D 20-Hz output is due to the large step size of the GFPE. At 20 Hz, with a reference sound speed of around 340 m/s, the wavelength is about 17 m. The step size used by the GFPE was about 15 wavelengths, which equates to around 255 m. At low frequencies, there is a tradeoff between speed and resolution in the GFPE.

Figures 10 and 11 show the same results as figures 8 and 9, for a frequency of 100 Hz. Figures 13 and 14 and 15 and 16 represent the GFPE and FFP outputs

at frequencies of 20 and 100 Hz, respectively, for the upward-refracting profile of figure 12. As with figure 7, this is an artificial profile. The source height is again 5 m.

The profile of figure 17 represents an actual surface duct calculated from temperature and wind measurements. Figures 18 and 19 show the GFPE output for this profile at 20 and 100 Hz, with a source height of 5 m. Figure 20 shows another profile for an actual surface duct. Figure 21 shows the corresponding GFPE output at 20 Hz. Note that these profiles actually contain multiple ducts near the surface, giving rise to a fairly complex sound field.

Finally, figure 22 shows an actual upper-air duct profile with the GFPE output at 50 Hz. In figure 23, the source height is 500 m, very close to the local minimum in the profile. This tends to somewhat focus the sound energy. Also note the shadow zone at the surface beyond 8 km.

As mentioned in the introduction, a parameter-sensitivity study was conducted on the GFPE. The technical report for this study contains a detailed discussion of the input parameters and a much more extensive presentation of the GFPE output and comparisons with the FFP.

Figure 8. 2-D GFPE output for the sound speed profile of figure 7. Frequency is 20 Hz, source height is 5 m.

40
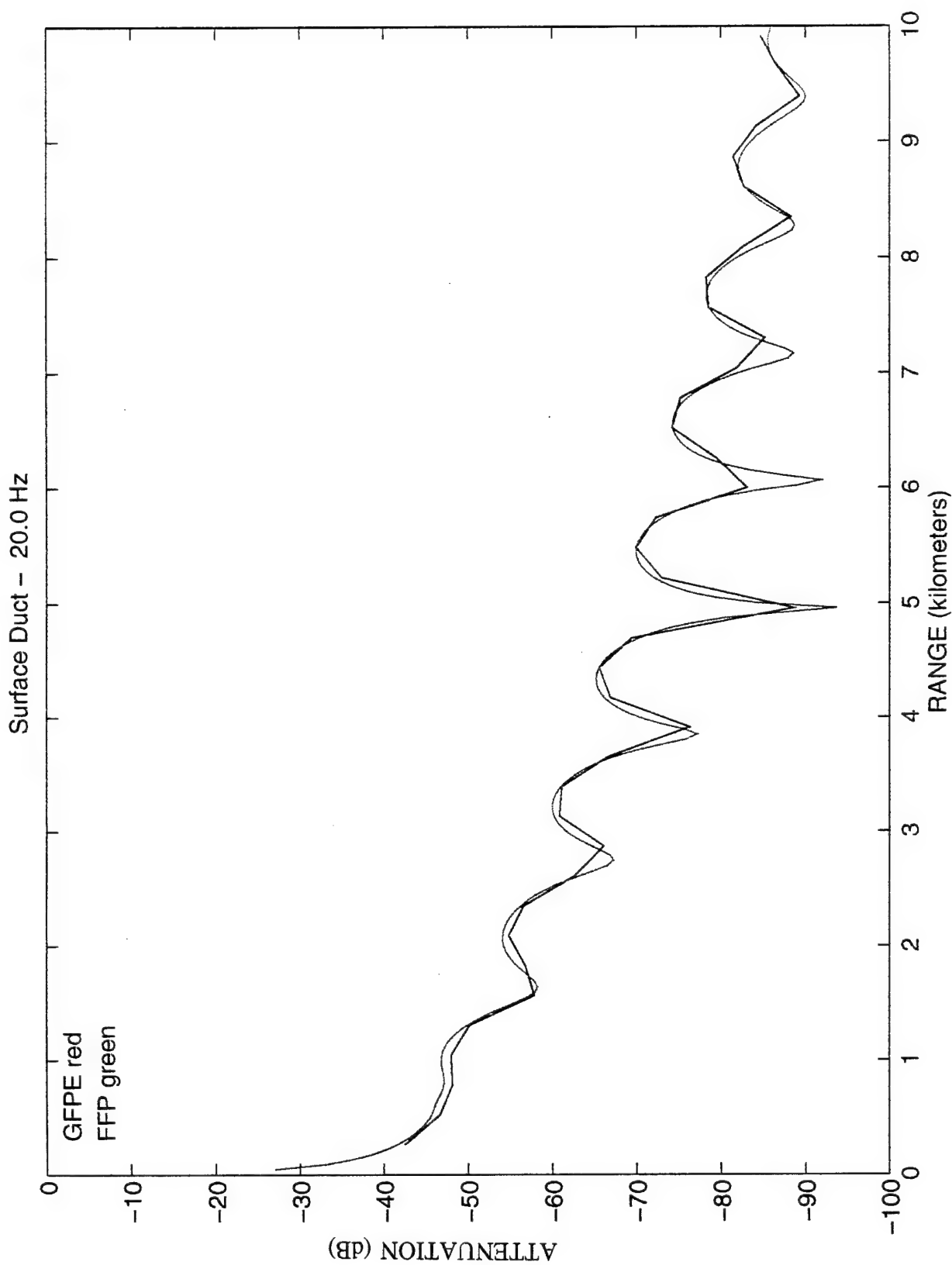
Figure 9. Comparison of 1-D GFPE and FFP outputs for the sound speed profile of figure 7. Frequency is 20 Hz, source height is 5 m.

41

Figure 10. 2-D GFPE output for the sound speed profile of figure 7. Frequency is 100 Hz, source height is 5 m.
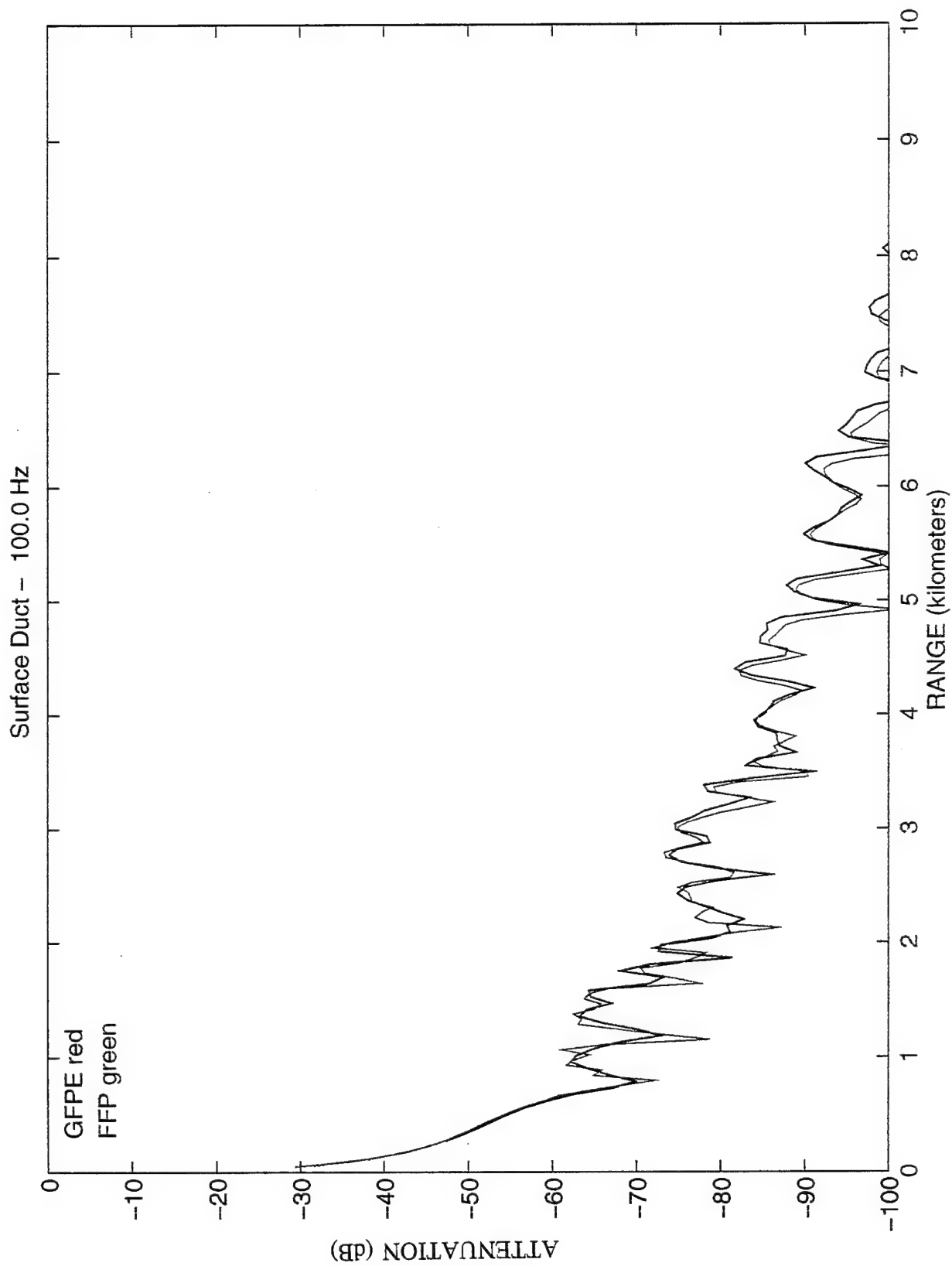
Figure 11. Comparison of 1-D GFPE and FFP output for the sound speed profile of figure 7. Frequency is 100 Hz, source height is 5 m.

43
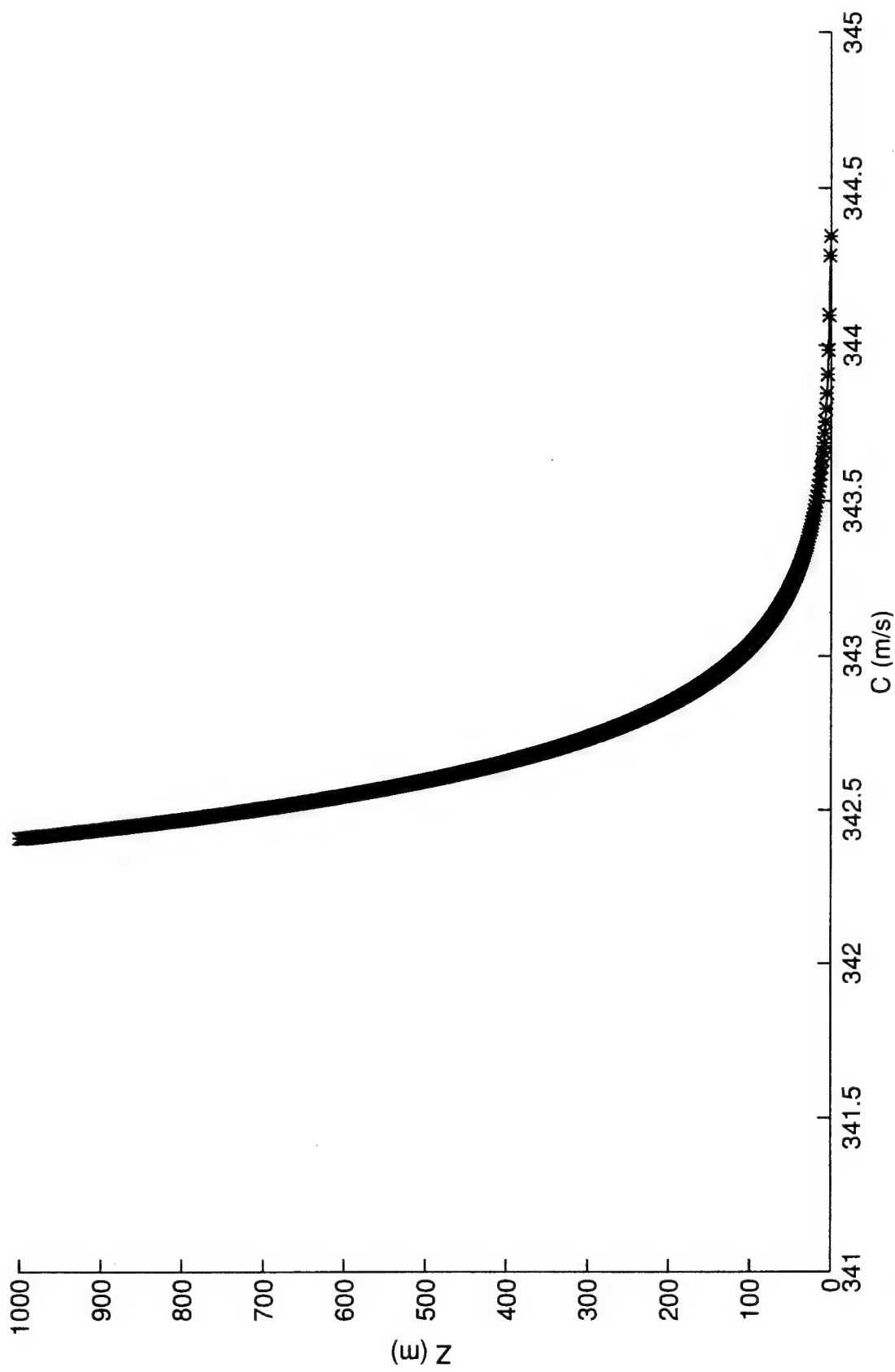
Figure 12. Upward refracting sound speed profile associated with figures 13 through 16.

44
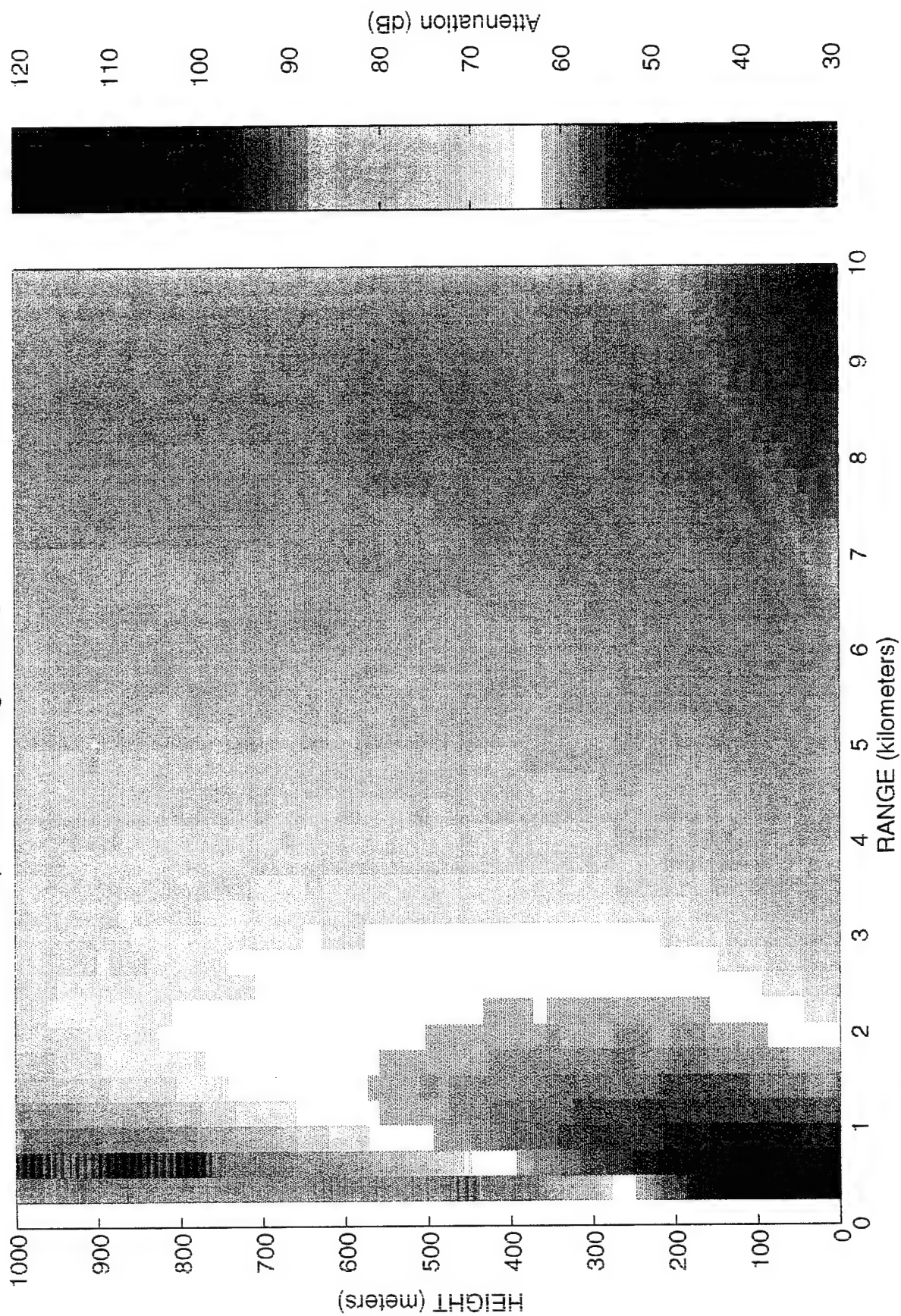
Figure 13. 2-D GFPE output for the sound speed profile of figure 12. Frequency is 20 Hz, source height is 5 m.

45
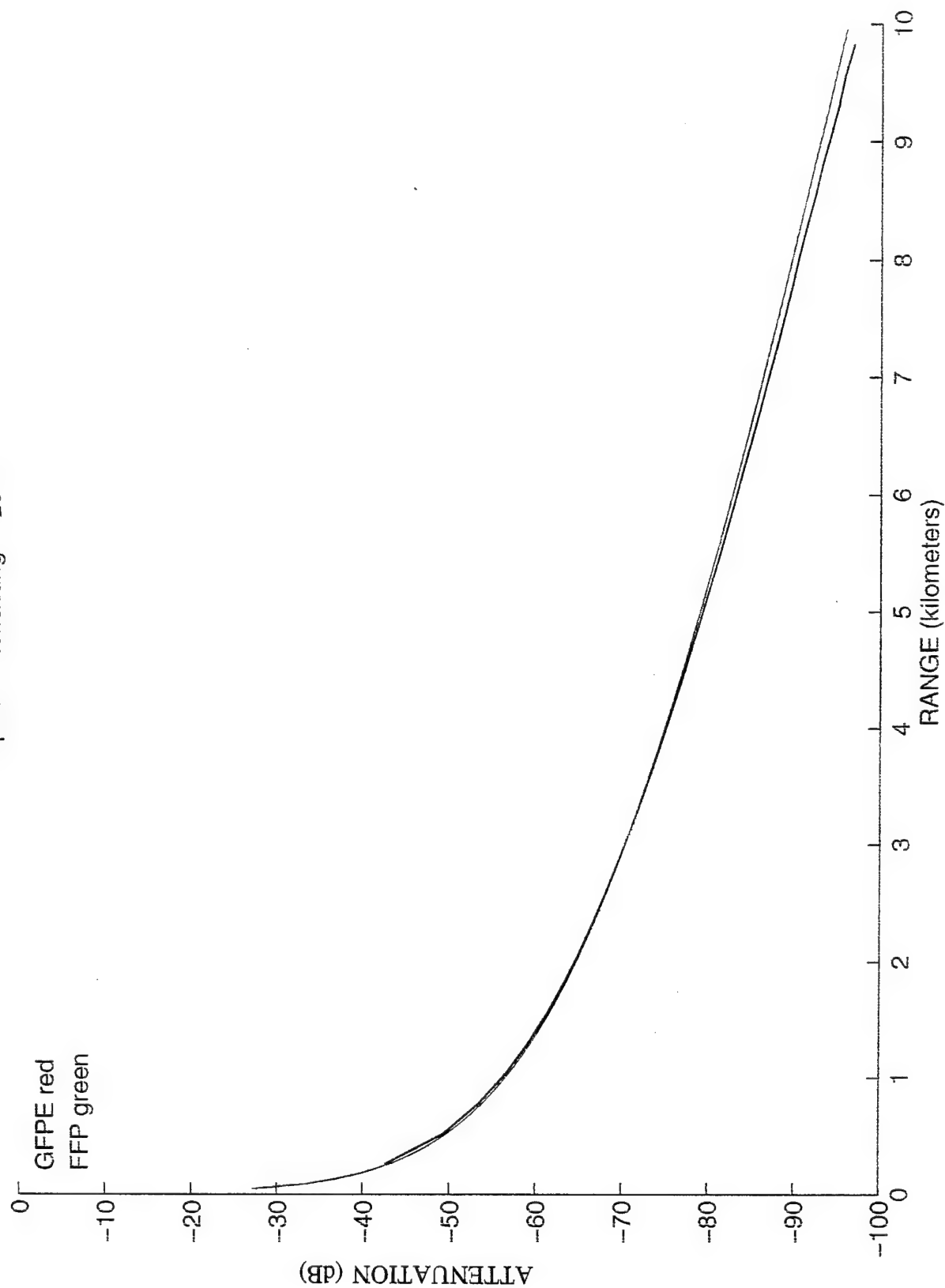
Figure 14. Comparison of 1-D GFPE and FFP output for the sound speed profile of figure 12. Frequency is 20 Hz, source height is 5 m.
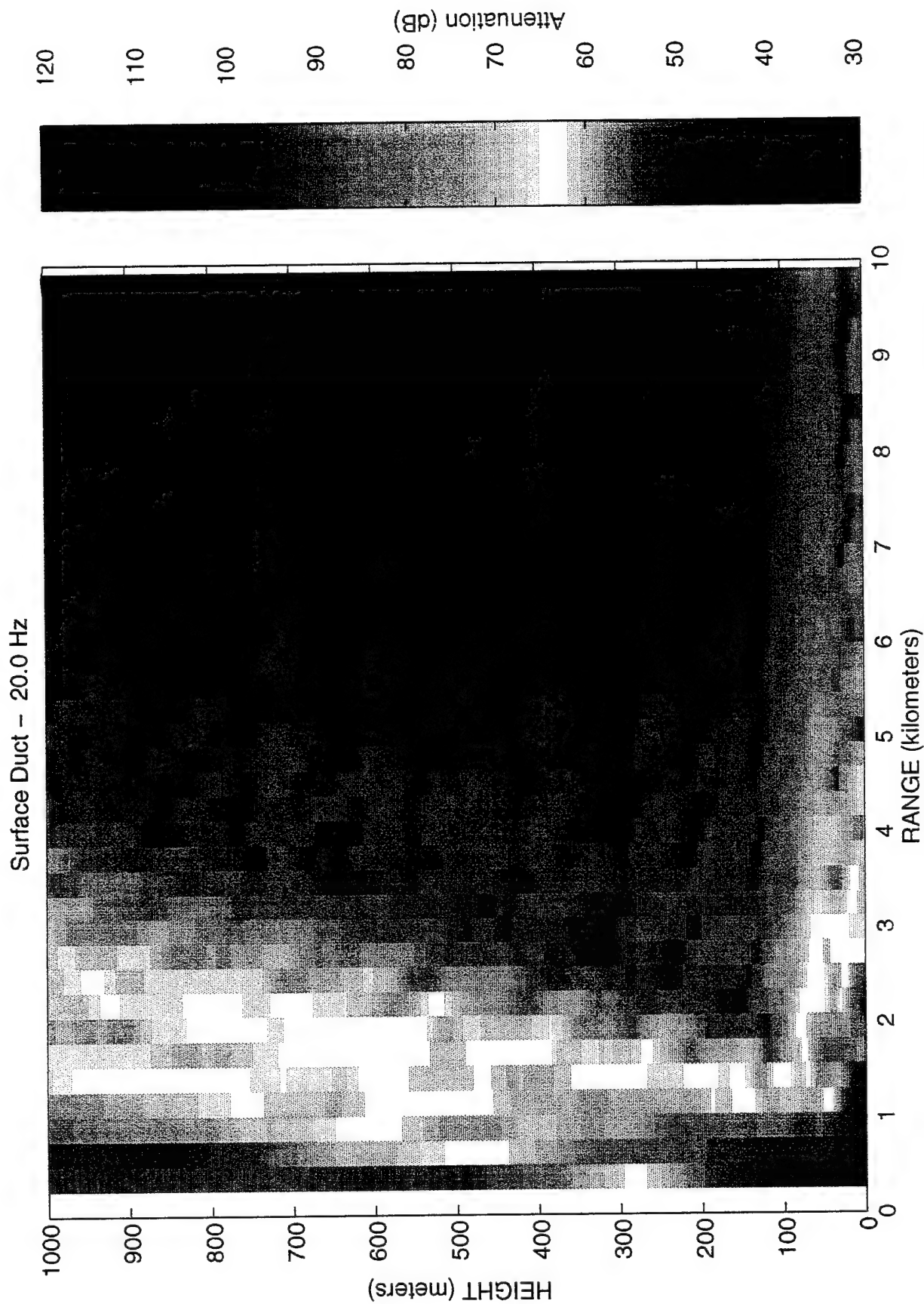
Figure 15. 2-D GFPE output for the sound speed profile of figure 12. Frequency is 100 Hz, source height is 5 m.
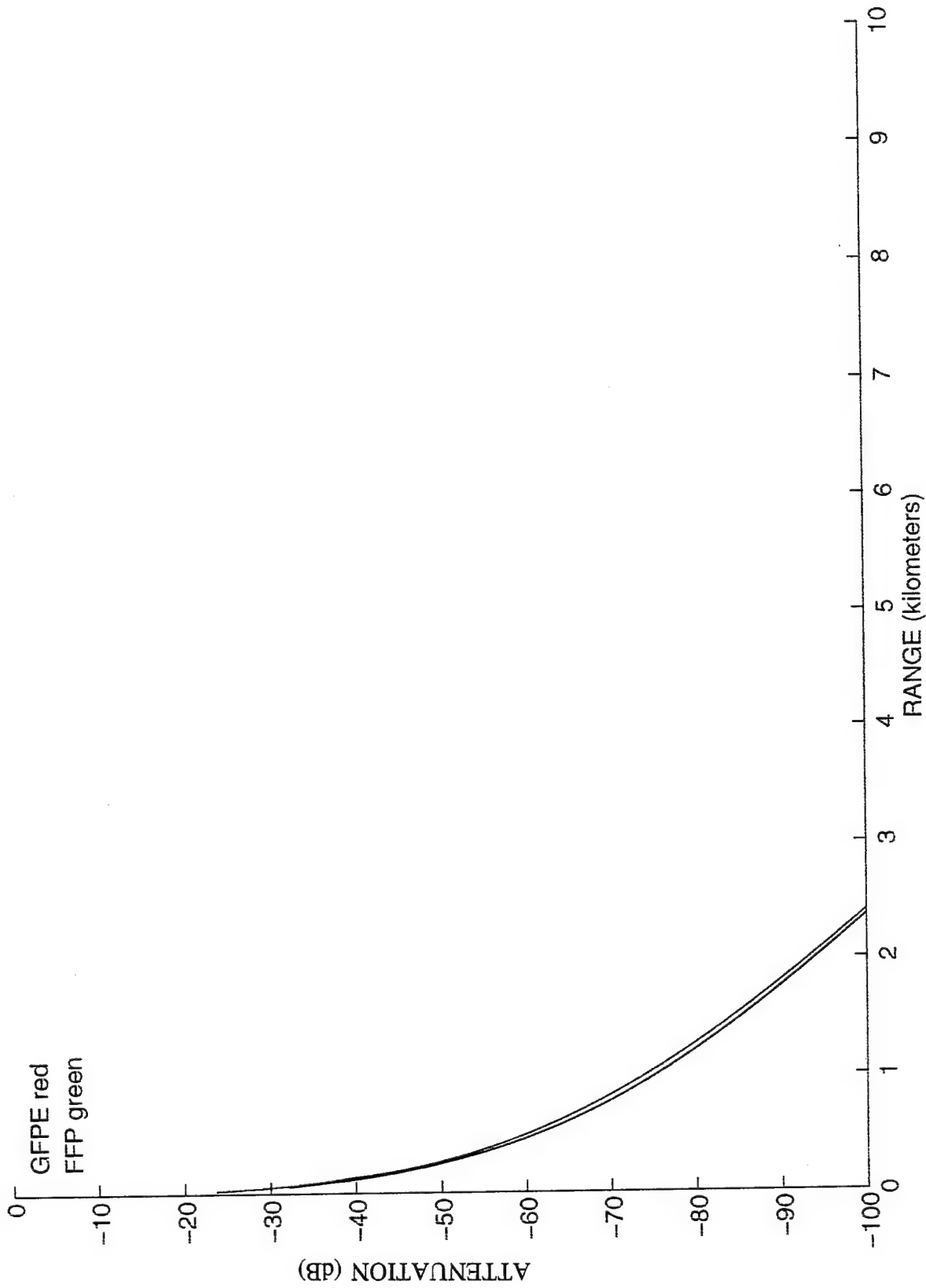
Figure 16. Comparison of GFPE and FFP 1-D outputs using the sound speed profile of figure 12. Frequency is 100 Hz, source height is 5 m.

48

e200910 Sound Speed
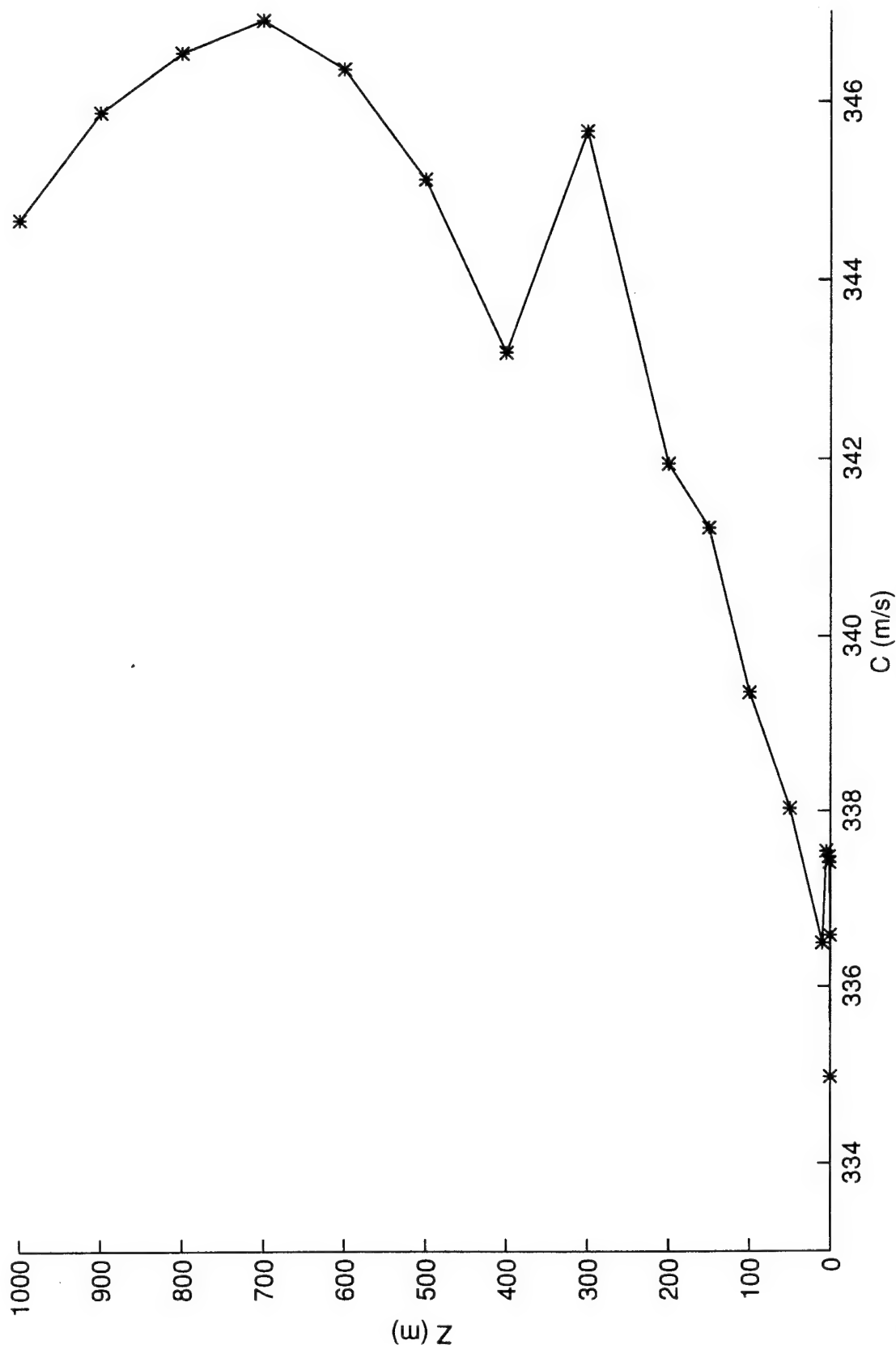
Figure 17. Measured surface duct sound speed profile associated with figures 18 and 19.

49
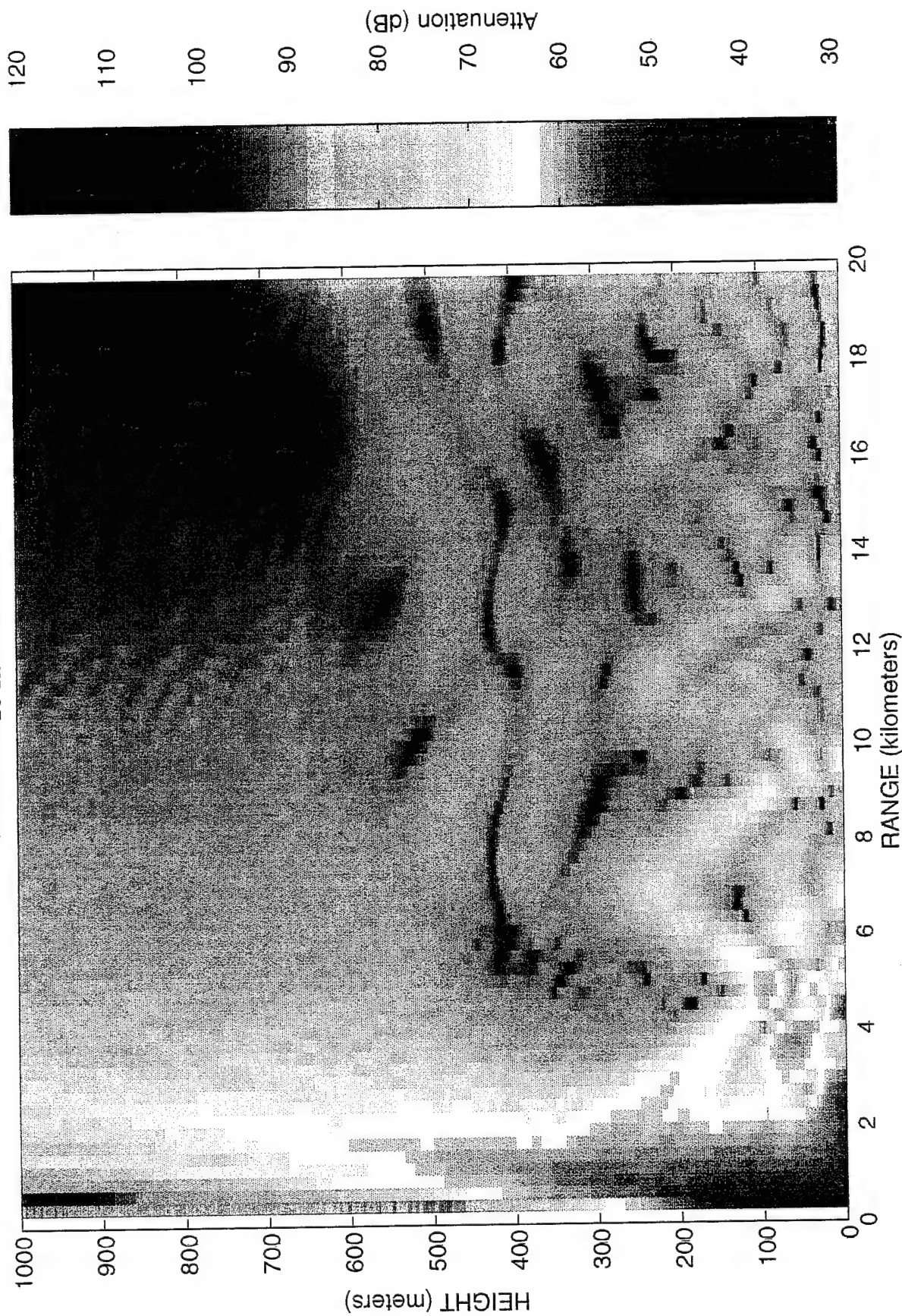
Figure 18. 2-D GFPE output using the sound speed profile of figure 17. Frequency is 20 Hz, source height is 5 m.

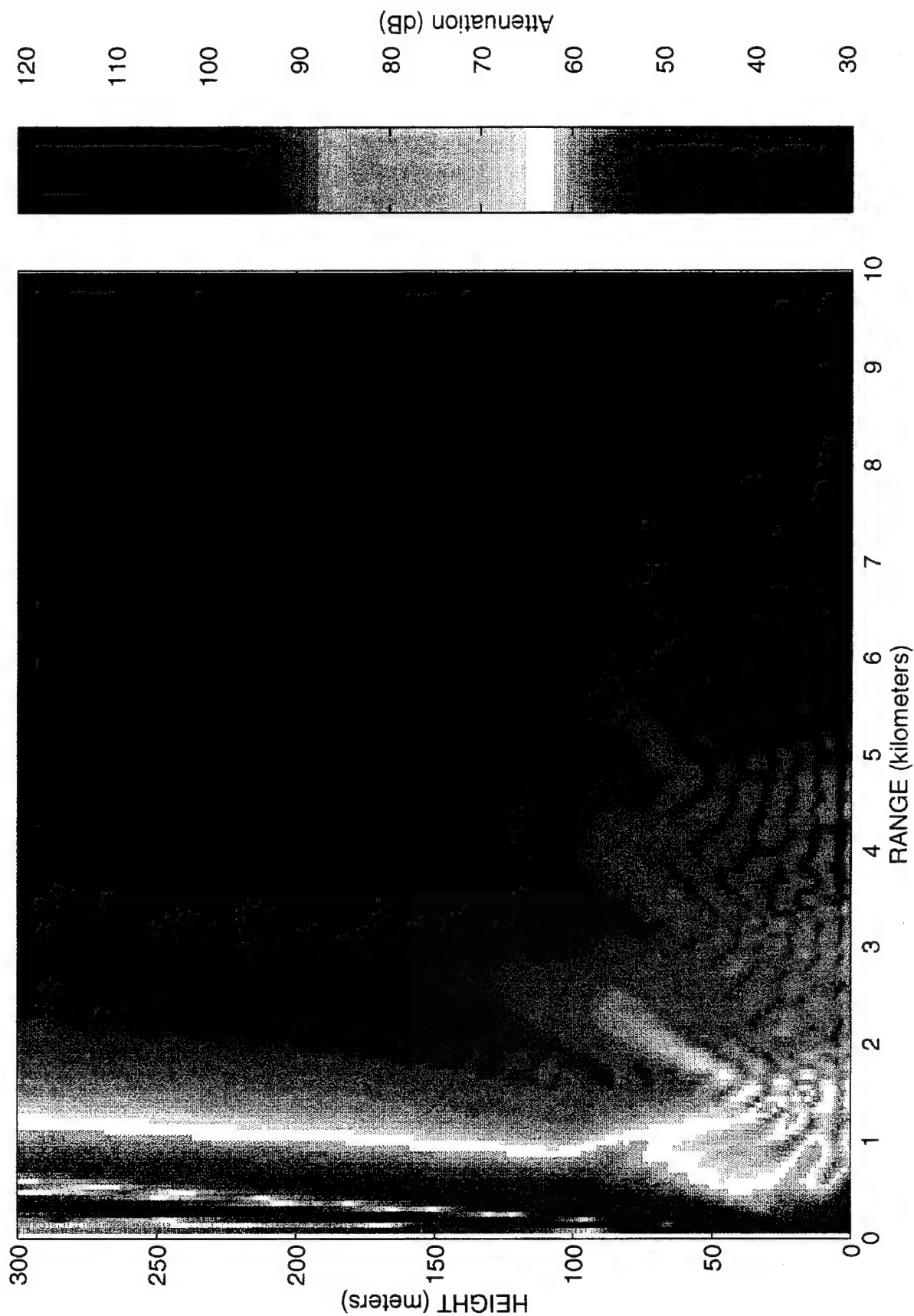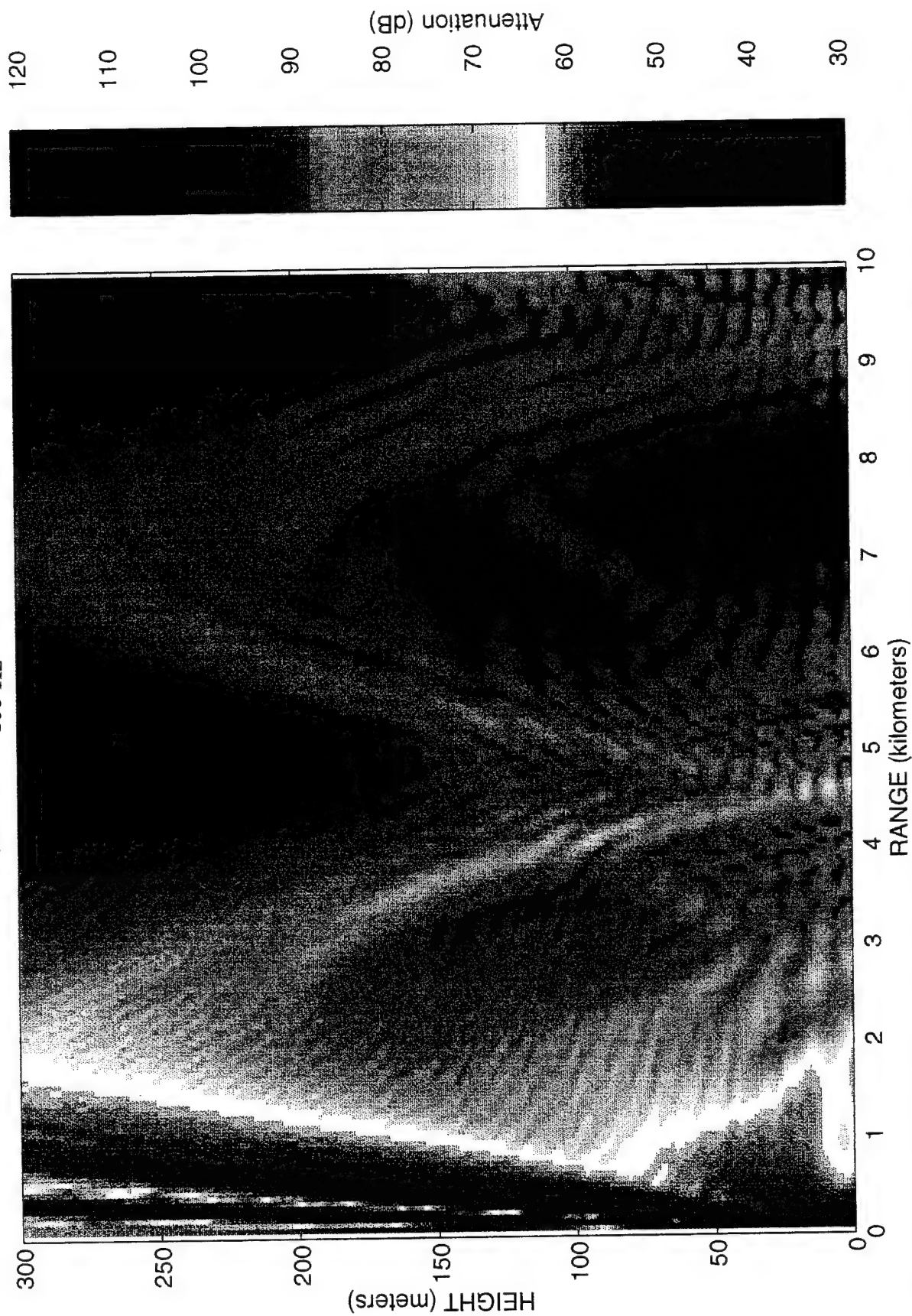**Figure 19. 2-D GFPE output for the sound speed profile of figure 17. Frequency is 100 Hz, source height is 5 m.**

51
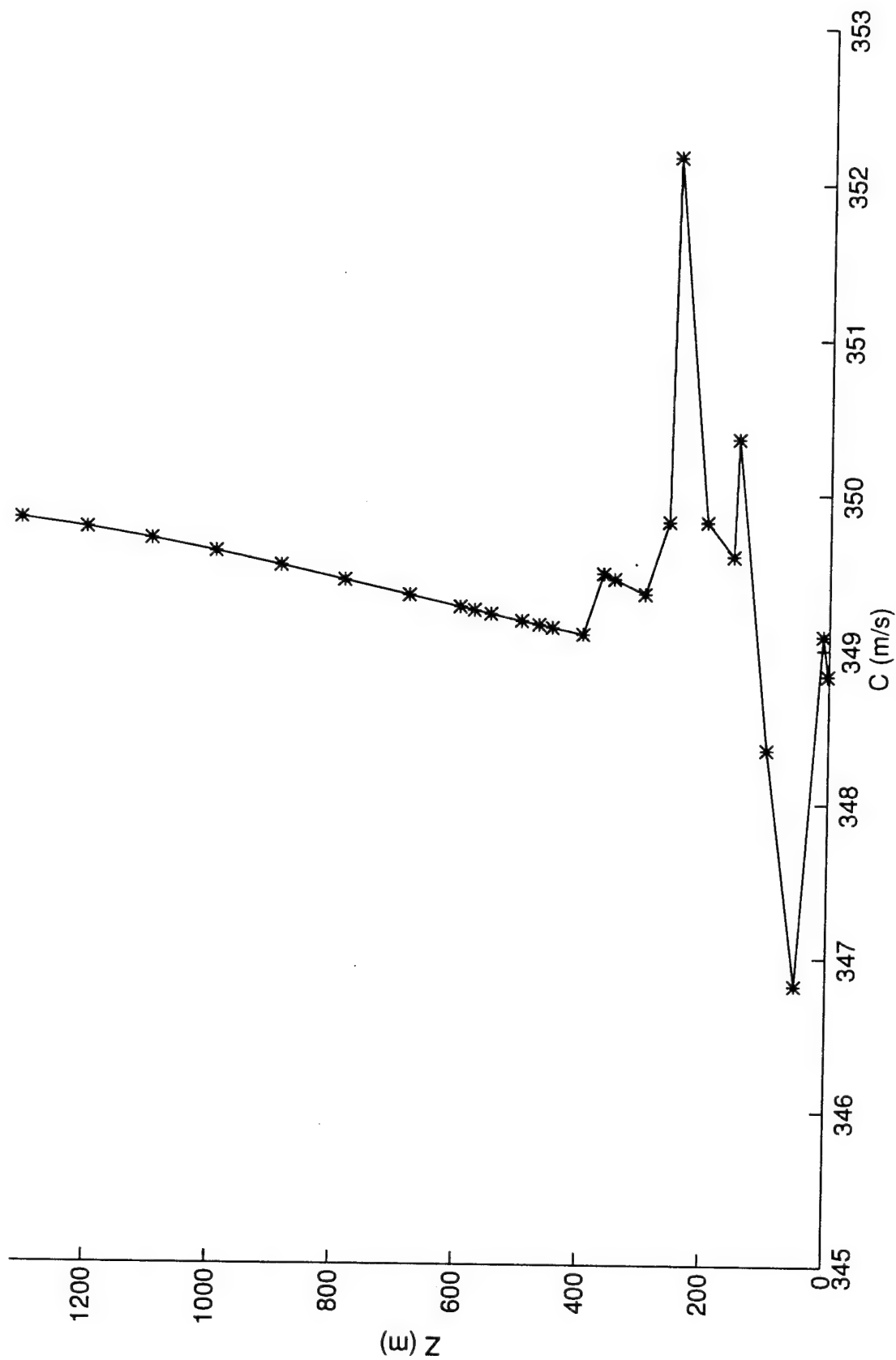
Figure 20. Measured surface duct sound speed profile associated with figure 21.

52
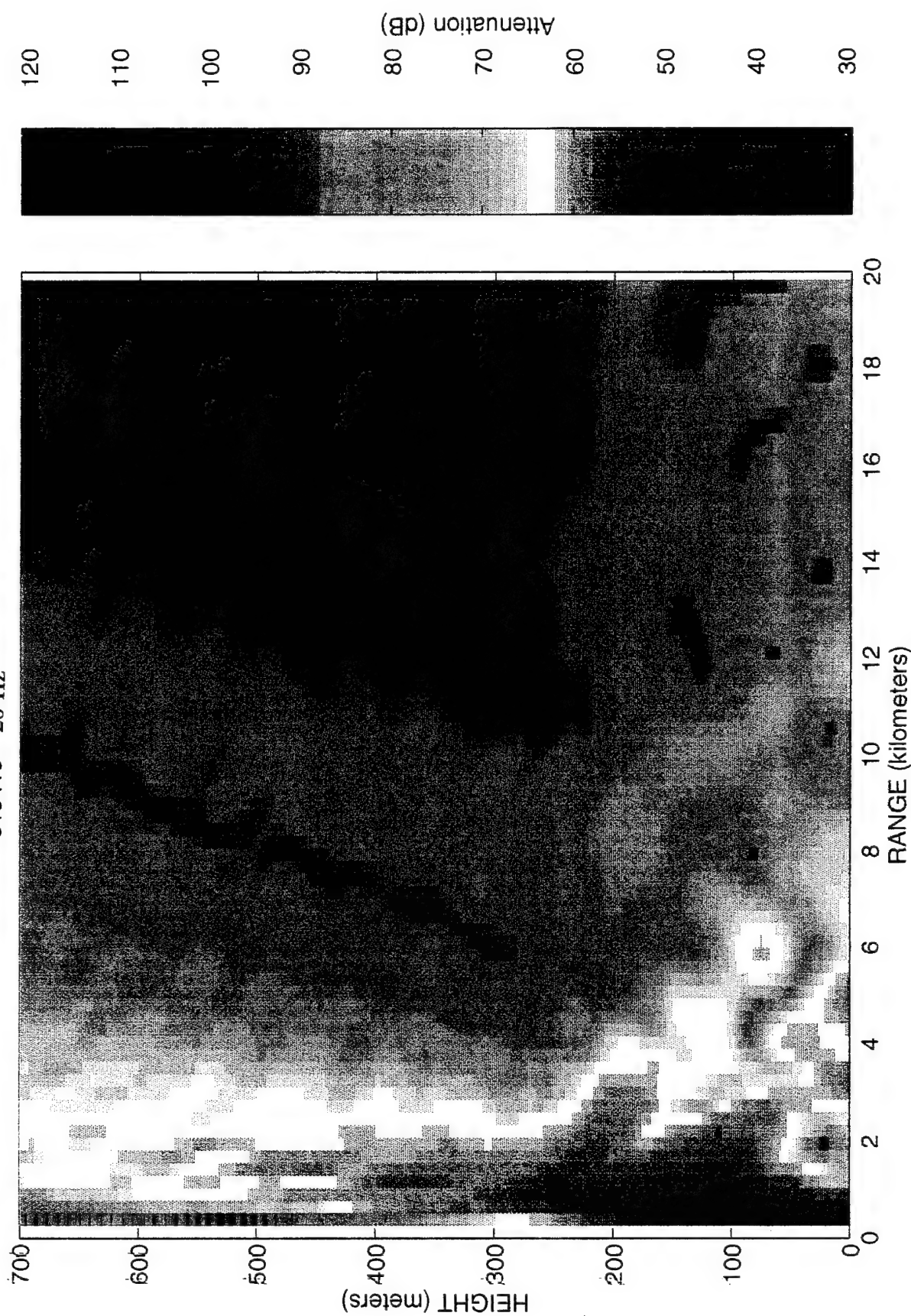
Figure 21. 2-D GFPE output using sound speed profile of figure 20. Frequency is 20 Hz, source height is 5 m.

53
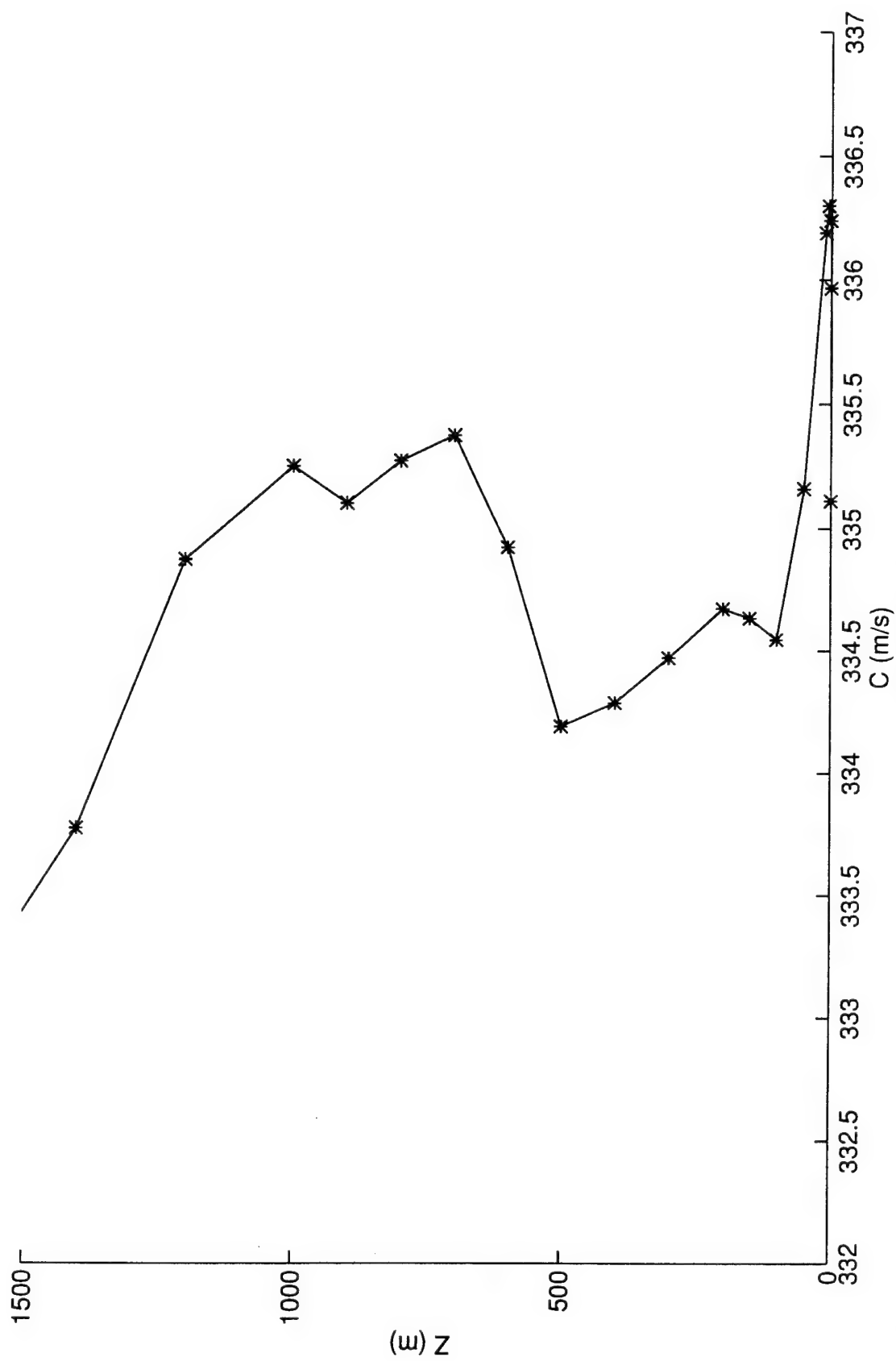
Figure 22. Measured upper-air duct sound speed profile associated with figure 23.

54
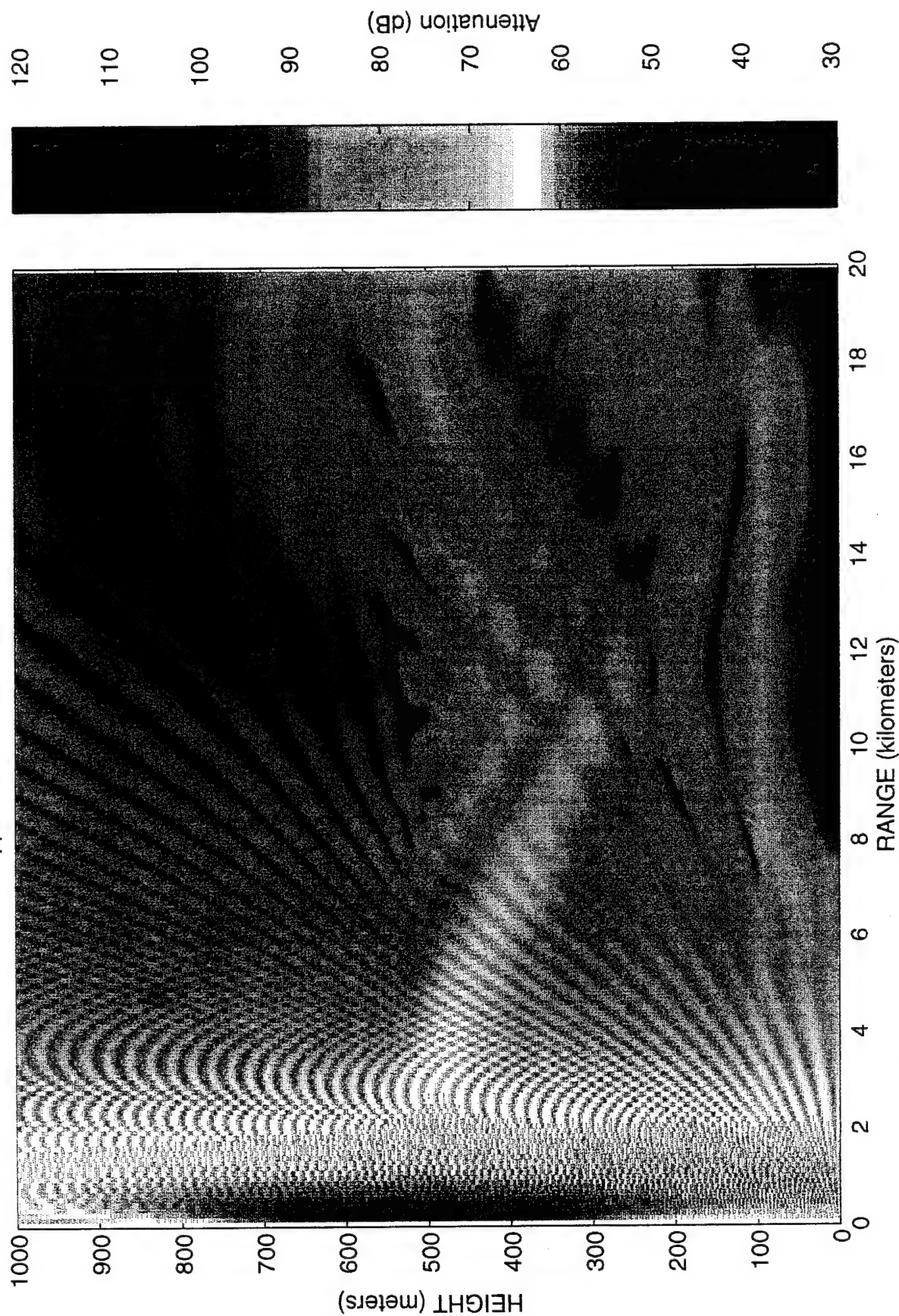
Figure 23. 2-D GFPE output using the sound speed profile of figure 22. Frequency is 50 Hz, source height is 500 m.

References

1. Tappert, F. D., and R. H. Hardin, "Computer Simulation of Long-Range Ocean Acoustic Propagation Using the Parabolic Equation Method," In *Proceedings of the 8th International Congress on Acoustics*, Goldcrest, London, 1974.

2. Fock, V. A., *Electromagnetic Diffraction and Propagation Problems*, 37 Pergamon Press, New York, 1965.

3. Di, X., and K. E. Gilbert, *A Survey of Acoustic Propagation Predictions for Realistic Atmospheres*, final report (DAAL03-91-C-0034), U.S. Army Research Office, Research Triangle Park, NC, 1992.

4. Dunford, N., and J. T. Schwartz, *Linear Operators, Part I*, Interscience Publishers, Inc., New York, 1958.

5. Fleck, J. A., J. R. Morris, and M. D. Feit, "Time-Dependant Propagation of High Energy Laser Beams Through the Atmosphere," *Applied Physics*, **10**, p 129-160, 1976.

6. Tappert, F. D., "The Parabolic Approximation Method," In *Wave Propagation and Underwater Acoustics*, ed. J. B. Keller and J. S. Papadakis, Springer-Verlag, New York, 1977.

7. Feit, M. D., and J. A. Fleck, Jr., "Light Propagation in Graded-Index Optical Fibers," *Applied Optics*, **17**, p 3990-3998, 1978.

8. Thompson, D. J., and N. R. Chapman, "A Wide-Angle, Split-Step Algorithm for the Parabolic Equation," *Journal of the Acoustical Society of America*, **74**, p 1848-1854, 1983.

9. McDaniel, S. T., "Propagation of a Normal Mode in the Parabolic Approximation," *Journal of the Acoustical Society of America*, **57**, p 307-311, 1975.

10. Attenborough, K., "Acoustical Impedance Models for Outdoor Ground Surfaces," *Journal of Sound and Vibration,* **99**, p 521-544, 1985.

11. Delaney, M. E., and E. N. Bazley, "Acoustical Properties of Fibrous Absorbent Material," *Applied Acoustics,* **3**, 105, p 116, 1970.

12. Pierce, A. D., "Acoustics, An Introduction to Its Physical Principles and Applications," *Acoustical Society of America,* Woodbury, NY, 1989.

13. Lee, S. W., et al., "Impedance Formulation of the Fast Field Program for Acoustic Wave Propagation in the Atmosphere," *Journal of the Acoustical Society of America,* **79**, p 628-634, 1986.

Acronyms and Abbreviations

FFP	Fast Field Program
FFT	Fast Fourier Transform
GFPE	Green's function parabolic equation
1-D	one-dimensional
PE	parabolic equation
2-D	two-dimensional

Distribution

	Copies
ARMY CHEMICAL SCHOOL ATZN CM CC ATTN MR BARNES FT MCCLELLAN AL 36205-5020	1
NASA MARSHAL SPACE FLT CTR ATMOSPHERIC SCIENCES DIV E501 ATTN DR FICHTL HUNTSVILLE AL 35802	1
NASA SPACE FLT CTR ATMOSPHERIC SCIENCES DIV CODE ED 41 1 HUNTSVILLE AL 35812	1
ARMY STRAT DEFNS CMND CSSD SL L ATTN DR LILLY PO BOX 1500 HUNTSVILLE AL 35807-3801	1
ARMY MISSILE CMND AMSMI RD AC AD ATTN DR PETERSON REDSTONE ARSENAL AL 35898-5242	1
ARMY MISSILE CMND AMSMI RD AS SS ATTN MR H F ANDERSON REDSTONE ARSENAL AL 35898-5253	1
ARMY MISSILE CMND AMSMI RD AS SS ATTN MR B WILLIAMS REDSTONE ARSENAL AL 35898-5253	1

```
ARMY MISSILE CMND                                        1
AMSMI RD DE SE
ATTN MR GORDON LILL JR
REDSTONE ARSENAL
AL 35898-5245

ARMY MISSILE CMND                                        1
REDSTONE SCI INFO CTR
AMSMI RD CS R DOC
REDSTONE ARSENAL
AL 35898-5241

ARMY MISSILE CMND                                        1
AMSMI
REDSTONE ARSENAL
AL 35898-5253

ARMY INTEL CTR                                           1
AND FT HUACHUCA
ATSI CDC C
FT HUACHUCA AZ 85613-7000

NAVAL WEAPONS CTR                                        1
CODE 3331
ATTN DR SHLANTA
CHINA LAKE CA 93555

PACIFIC MISSILE TEST CTR                                 1
GEOPHYSICS DIV
ATTN CODE 3250
POINT MUGU CA 93042-5000

LOCKHEED MIS & SPACE CO                                  1
ATTN KENNETH R HARDY
ORG 91 01 B 255
3251 HANOVER STREET
PALO ALTO CA 94304-1191

NAVAL OCEAN SYST CTR                                     1
CODE 54
ATTN DR RICHTER
SAN DIEGO CA 92152-5000
```

METEOROLOGIST IN CHARGE   1
KWAJALEIN MISSILE RANGE
PO BOX 67
APO SAN FRANCISCO
CA 96555

DEPT OF COMMERCE CTR   1
MOUNTAIN ADMINISTRATION
SPPRT CTR LIBRARY R 51
325 S BROADWAY
BOULDER CO 80303

DR HANS J LIEBE   1
NTIA ITS S 3
325 S BROADWAY
BOULDER CO 80303

NCAR LIBRARY SERIALS   1
NATL CTR FOR ATMOS RSCH
PO BOX 3000
BOULDER CO 80307-3000

DEPT OF COMMERCE CTR   1
325 S BROADWAY
BOULDER CO 80303

DAMI POI   1
WASH DC 20310-1067

MIL ASST FOR ENV SCI OFC   1
OF THE UNDERSEC OF DEFNS
FOR RSCH & ENGR R&AT E LS
PENTAGON ROOM 3D129
WASH DC 20301-3080

DEAN RMD   1
ATTN DR GOMEZ
WASH DC 20314

ARMY INFANTRY   1
ATSH CD CS OR
ATTN DR E DUTOIT
FT BENNING GA 30905-5090

AIR WEATHER SERVICE   1
TECH LIBRARY FL4414 3
SCOTT AFB IL 62225-5458

USAFETAC DNE   1
ATTN MR GLAUBER
SCOTT AFB IL 62225-5008

HQ AWS DOO 1   1
SCOTT AFB IL 62225-5008

ARMY SPACE INSTITUTE   1
ATTN ATZI SI 3
FT LEAVENWORTH
KS 66027-5300

PHILLIPS LABORATORY   1
PL LYP
ATTN MR CHISHOLM
HANSCOM AFB MA 01731-5000

ATMOSPHERIC SCI DIV   1
GEOPHYSICS DIRCTRT
PHILLIPS LABORATORY
HANSCOM AFB MA 01731-5000

PHILLIPS LABORATORY   1
PL LYP 3
HANSCOM AFB MA 01731-5000

RAYTHEON COMPANY   1
ATTN DR SONNENSCHEIN
528 BOSTON POST ROAD
SUDBURY MA 01776
MAIL STOP 1K9

ARMY MATERIEL SYST   1
ANALYSIS ACTIVITY
AMXSY
ATTN MP H COHEN
APG MD 21005-5071

ARMY MATERIEL SYST   1
ANALYSIS ACTIVITY
AMXSY AT
ATTN MR CAMPBELL
APG MD 21005-5071

ARMY MATERIEL SYST
ANALYSIS ACTIVITY
AMXSY CR
ATTN MR MARCHET
APG MD 21005-5071

1

ARL CHEMICAL BIOLOGY
NUC EFFECTS DIV
AMSRL SL CO
APG MD 21010-5423

1

ARMY MATERIEL SYST
ANALYSIS ACTIVITY
AMXSY
APG MD 21005-5071

1

NAVAL RESEARCH LABORATORY
CODE 4110
ATTN MR RUHNKE
WASH DC 20375-5000

1

ARMY MATERIEL SYST
ANALYSIS ACTIVITY
AMXSY CS
ATTN MR BRADLEY
APG MD 21005-5071

1

ARMY RESEARCH LABORATORY
AMSRL D
2800 POWDER MILL ROAD
ADELPHI MD 20783-1145

1

ARMY RESEARCH LABORATORY
AMSRL OP SD TP
TECHNICAL PUBLISHING
2800 POWDER MILL ROAD
ADELPHI MD 20783-1145

1

ARMY RESEARCH LABORATORY
AMSRL OP CI SD TL
2800 POWDER MILL ROAD
ADELPHI MD 20783-1145

1

```
ARMY RESEARCH LABORATORY                                          1
AMSRL SS SH
ATTN DR SZTANKAY
2800 POWDER MILL ROAD
ADELPHI MD 20783-1145

ARMY RESEARCH LABORATORY                                          1
AMSRL
2800 POWDER MILL ROAD
ADELPHI MD 20783-1145

NATIONAL SECURITY AGCY W21                                        1
ATTN DR LONGBOTHUM
9800 SAVAGE ROAD
FT GEORGE G MEADE
MD 20755-6000

OIC NAVSWC                                                        1
TECH LIBRARY CODE E 232
SILVER SPRINGS
MD 20903-5000

ARMY RSRC OFC                                                     1
ATTN DRXRO GS
PO BOX 12211
RTP NC 27009

DR JERRY DAVIS                                                    1
NCSU
PO BOX 8208
RALEIGH NC 27650-8208

ARMY CCREL                                                        1
CECRL GP
ATTN DR DETSCH
HANOVER NH 03755-1290

ARMY ARDEC                                                        1
SMCAR IMI I BLDG 59
DOVER NJ 07806-5000

ARMY SATELLITE COMM AGCY                                          1
DRCPM SC 3
FT MONMOUTH NJ 07703-5303
```

66

ARMY COMMUNICATIONS   1
ELECTR CTR FOR EW RSTA
AMSEL EW D
FT MONMOUTH NJ 07703-5303

ARMY COMMUNICATIONS   1
ELECTR CTR FOR EW RSTA
AMSEL EW MD
FT MONMOUTH NJ 07703-5303

ARMY DUGWAY PROVING GRD   1
STEDP MT DA L 3
DUGWAY UT 84022-5000

ARMY DUGWAY PROVING GRD   1
STEDP MT M
ATTN MR BOWERS
DUGWAY UT 84022-5000

DEPT OF THE AIR FORCE   1
OL A 2D WEATHER SQUAD MAC
HOLLOMAN AFB
NM 88330-5000

PL WE   1
KIRTLAND AFB NM
87118-6008

USAF ROME LAB TECH   1
CORRIDOR W STE 262 RL SUL
26 ELECTR PKWY BLD 106
GRIFFISS AFB
NY 13441-4514

AFMC DOW   1
WRIGHT PATTERSON AFB
OH 0334-5000

ARMY FIELD ARTLLRY SCHOOL   1
ATSF TSM TA
FT SILL OK 73503-5600

NAVAL AIR DEV CTR   1
CODE 5012
ATTN AL SALIK
WARMINISTER PA 18974

ARMY FOREGN SCI TECH CTR 1
CM
220 7TH STREET NE
CHARLOTTESVILLE
VA 22901-5396

NAVAL SURFACE WEAPONS CTR 1
CODE G63
DAHLGREN VA 22448-5000

ARMY OEC 1
CSTE EFS
PARK CENTER IV
4501 FORD AVE
ALEXANDRIA VA 22302-1458

ARMY CORPS OF ENGRS 1
ENGR TOPOGRAPHICS LAB
ETL GS LB
FT BELVOIR VA 22060

TAC DOWP 1
LANGLEY AFB
VA 23665-5524

ARMY TOPO ENGR CTR 1
CETEC ZC 1
FT BELVOIR VA 22060-5546

LOGISTICS CTR 1
ATCL CE
FT LEE VA 23801-6000

SCI AND TECHNOLOGY 1
101 RESEARCH DRIVE
HAMPTON VA 23666-1340

ARMY NUCLEAR CML AGCY 1
MONA ZB BLDG 2073
SPRINGFIELD VA 22150-3198

ARMY FIELD ARTLLRY SCHOOL 1
ATSF F FD
FT SILL OK 73503-5600

USATRADOC   1
ATCD FA
FT MONROE VA 23651-5170

ARMY TRADOC ANALYSIS CTR   1
ATRC WSS R
WSMR NM 88002-5502

ARMY RESEARCH LABORATORY   1
AMSRL BE M
BATTLEFIELD ENVIR DIR
WSMR NM 88002-5501

ARMY RESEARCH LABORATORY   1
AMSRL BE A
BATTLEFIELD ENVIR DIR
WSMR NM 88002-5501

ARMY RESEARCH LABORATORY   1
AMSRL BE W
BATTLEFIELD ENVIR DIR
WSMR NM 88002-5501

ARMY RESEARCH LABORATORY   1
AMSRL BE
ATTN MR VEAZEY
BATTLEFIELD ENVIR DIR
WSMR NM 88002-5501

DEFNS TECH INFO CTR   1
CENTER DTIC BLS
BLDG 5 CAMERON STATION
ALEXANDRIA
VA 22304-6145

ARMY MISSILE CMND   1
AMSMI
REDSTONE ARSENAL
AL 35898-5243

ARMY DUGWAY PROVING GRD   1
STEDP 3
DUGWAY UT 84022-5000

USATRADOC   1
ATCD FA
FT MONROE VA 23651-5170

ARMY FIELD ARTLRY SCHOOL ATSF FT SILL OK 73503-5600	1
WSMR TECH LIBRARY BR STEWS IM IT WSMR NM 88001	1
Record Copy	10
Total	93